МІНІСТЕРСТВО ОСВІТИ І НАУКИ, МОЛОДІ ТА СПОРТУ УКРАЇНИ
НАЦІОНАЛЬНИЙ ТЕХНІЧНИЙ УНІВЕРСИТЕТ УКРАЇНИ
"КИЇВСЬКИЙ ПОЛІТЕХНІЧНИЙ ІНСТИТУТ"

_____Механіко-машинобудівний інститут_____
(назва факультету, інституту)

_____Динаміки і міцності машин та опору матеріалів_____
(назва кафедри)

"На правах рукопису"   «До захисту допущено»
УДК_____   Завідувач кафедри
                                                          _____Піскунов С.О.
                                                          (підпис)   (ініціали, прізвище)

                                                          "___" _____20___р.

МАГІСТЕРСЬКА ДИСЕРТАЦІЯ

зі спеціальності _131 Прикладна механіка_____
(код та назва спеціальності)

_____

на тему: Напружено-деформований стан в зоні вершини магістральної

тріщини в обшивці фюзеляжу пасажирського літака

Студент групи МП-83мп   Кучер Анастасія Євгеніївна   _____

        (шифр групи)   (прізвище, ім'я, по батькові)   (підпис)

Науковий керівник д.т.н.,проф.   Бабенко А. Є. .   _____
                (вчені ступінь та звання, прізвище, ініціали)

Консультанти: (за рішенням кафедри)

Київ 2019

ABSTRACT

Національний технічний університет України

«Київський політехнічний інститут ім. Ігоря Сікорського»

Факультет (інститут)＿＿＿＿＿＿Механіко-машинобудівний інститут＿＿＿＿＿.

<div align="center">(повна назва)</div>

Кафедра＿＿＿＿＿Динаміки і міцності машин та опору матеріалів＿＿＿＿.

<div align="center">(повна назва)</div>

Освітньо-кваліфікаційний рівень «магістр»

Напрям підготовки ＿＿＿＿＿6.050501 Прикладна механіка＿＿＿＿＿＿.

<div align="center">(код і назва)</div>

Спеціальність ＿＿＿＿8.05050101 Динаміка і міцність машин＿＿＿＿＿.

<div align="center">(код і назва)</div>

<div align="right">

ЗАТВЕРДЖУЮ

Завідувач кафедри

＿＿＿＿＿＿＿ С.О. Пискунов

(підпис)　　(ініціали, прізвище)

« _» ＿＿＿＿＿2019 р.

</div>

ЗАВДАННЯ

на магістерську дисертацію студенту

＿＿＿＿＿＿＿＿＿＿Кучер Анастасії Євгеніївні＿＿＿＿＿＿＿＿＿.

<div align="center">(прізвище, ім'я, по батькові)</div>

1. Тема дисертації ＿＿＿＿＿＿Напружено-деформований стан в зоні вершини магістральної тріщини в обшивці фюзеляжу пасажирського літака

науковий керівник дисертації＿д.т.н.,проф.＿Бабенко А. Є.＿＿＿＿＿ ＿ ,

<div align="center">(прізвище, ім'я, по батькові, науковий ступінь, вчене звання)</div>

затверджені наказом по університету від «＿＿» ＿＿＿＿ 2019 р. № ＿＿＿＿

2. Строк подання студентом дисертації: «＿＿» ＿＿＿＿ 2019 р

3. Об'єкт дослідження ＿пластина обшивки фюзеляжу пасажирського літака

4. Предмет дослідження ＿зріст тріщини＿＿＿＿＿＿＿＿＿＿＿＿＿＿＿

5. Перелік завдань, які потрібно розробити <u>змоделювати процес росту тріщини,</u>

<u>та обробку даних,</u>

6. Орієнтовний перелік ілюстративного матеріалу <u>   51 малюнок   </u>

_____

_____

7. Орієнтовний перелік публікацій <u>   </u> _____

_____

8. Консультанти розділів дисертації

Розділ	Прізвище, ініціали та посада консультанта	Підпис, дата	
		завдання видав	завдання прийняв

9. Дата видачі завдання: <u>02 вересня 2019 року</u>

<div align="center">Календарний план</div>

№ з/п	Назва етапів виконання магістерської дисертації	Строк виконання етапів магістерської дисертації	Примітка
1	Ознайомлення з літературою	02.09.19-01.10.19	Виконано
2	Вибір модельованого кісткового регенерату з полімерних матеріалів	01.10.19-15.10.19	Виконано
3	Визначення модулів пружності при різних сумішах полімеру	15.10.19-01.11.19	Виконано
4	Проведення випробувань на системі остеосинтезу	01.11.19-15.11.19	Виконано
5	Обробка експериментальних результатів	15.11.19-22.11.19	Виконано
6	Підготовка презентації по стану роботи	22.11.19-27.11.19	Виконано
7	Оформлення роботи	27.11.19-16.12.19	Виконано

Студент   _____   _____ Кучер А. Є .

<div align="center">(підпис)   (ініціали, прізвище)</div>

Науковий керівник дисертації   _____   _____ Бабенко А. Є..

<div align="center">(підпис)   (ініціали, прізвище)</div>

ABSTRACT

The master`s degree dissertation for the amount of work is 55 pages, 51 figures, 2 tables, and contains 7 literature.

The object of the work is the skin with main crack for passenger aircraft.

The main goal of this dissertation is to investigate the dependence of the geometric coefficient Y on the length of the crack l.

The investigate is done using semi-empirical methods. All calculations were carried out in Excel and COSMOS\M.

As a result of this work was investigated the dependence of the geometric coefficient Y on the length of the crack l.

Реферат

Дана магістерська дисертація за обсягом роботи складає 55 сторінки, 51 ілюстрація, 2 таблиць та містить 7 літературних джерел.

Об'єктом дослідження обшивка фюзеляжу пасажирського літака магістральною тріщиною

Головна ціль даної дисертації – дослідити залежність геометричного коефіцієнта Y від довжини тріщини l .

Дослідження виконано з використанням напівемпіричних методів. Всі розрахунки виконані в програмному комплексі Microsoft Excel та COSMOS\M.

В результаті цієї роботи була отримана залежність геометричного коефіцієнта Y від довжини тріщини l .

Contents

INTRODUCTION

The aircraft structural design processes depend on many factors such as customer and manufacturer demands, safety protocols, physical and economical constraints. The design process starts with aircraft's intended purpose. Commercial airliners are designed for carrying of passengers or cargo payload, long range and greater fuel efficiency, while fighters are designed to perform high speed and maneuverability. For all cases aircraft design is a compromise between many competing factors and constraints. For example, an aircraft must possess high strength and durability with minimum penalty of weight.

Strength of the aircraft construction is the main factor, which provides safety of flight, weight, in turn, directly influence fuel efficiency. Therefore, in order to obtain a high performance aircraft, its strength must be determined by the most efficient and sophisticated methods.

The object of structural design is to provide the structure that will permit the aircraft, whether military or civil, perform its functions most efficiently. Modern methods of strength assessment are based on experimental, empirical and theoretical experience.

The dissertation is devoted to the growth of fatigue cracks and shows the relationship between the crack length and other parameters. The first section describes the development of approaches to the design of aircraft describes each of them. The second section shows theoretical developments in the field of fatigue and methods for assessing crack growth. The modeling of this problem and the analysis results are shown in section 3. The processing of the experimental results and the desired dependences are shown in section 4.

Keywords: *crack, crack growth, stress intensity factor, Y-factor.*

1. DEVELOPMENT OF AIRCRAFT DESIGN

The design methods presently used for aeronautical structures must guarantee the absence of catastrophic failures for their operating life.

A first method was the Safe-Life - replacement of the component after an established life. This applies a safety factor to the mean life of the structure, but doubts can remain about the number of tests performed to establish the mean life and about the correctness of the safety factor because it doesn't consider the data scatter factor.

The Damage Tolerance approach – the structure must "tolerate" a crack until a planned maintenance action can find and repair it), [1], is based on the identification of the worst among the possible situations; the phenomena involved have a statistical nature, and the structure must be verified under the most critical condition.

A disadvantage concerned with this approach is that, by joining the probabilities of the more unfavourable events, an excessively low probability of failure (POF) results, appreciated from the safety point of view, but extremely penalising from the point of view of weights or costs.

With the development of reliable fracture mechanics analysistechniques, it became possible to relate detectable damage, damage growth, and critical damage size to establish inspection methods and frequency required to maintain safe operation. FAA regulations for damage tolerance were published in 1978 . Implementation of damage tolerance verification requirements encouraged application of contemporary engineering methods to determine inspection thresholds and intervals for fatigue inspection programs while complementing the use of fail safe design principles. Up-front use of these techniques in recent models has significantly influenced the design, including the structural arrangement, materials and stress levels, accessibility, inspectability, and repairability.

These techniques also enable development of candidate inspection techniques and intervals to ensure their feasibility and reliability when implemented at an appropriate threshold in the airplane service life.

In addition to residual strength evaluations, damage growth and inspection requirements with considerations of damage at multiple sites were incorporated in Amendment 45 of FAR 25.571 for new airplanes and in CAA Notice 89 and AC 91-56 for of supplemental inspections of aging airplanes.

Damage tolerance is the ability of structure to sustain regulatory loads in the presence of unknown fatigue, corrosion, or accidental damage until such damage is detected through inspections or malfunctions and is repaired. All primary flight-loaded structure must be designed to be damage tolerant. This requires that the structure have sufficient damage growth properties and detection characteristics so that if damage were to develop at single or multiple sites, normal specified airline inspections would ensure that the damage is found before the crack reduces the residual strength capability of the structure below limit load. This requirement, in conjunction with the fail safe requirements is essential to provide the most comprehensive assurance of continued safety throughout the service life of an airplane.

All primary structure must be designed to be damage tolerant, as described in FAR 25.571(c) . Damage detection by being obvious and/or evident is preferable to damage detection by planned inspection for maintaining residual strength capability.

Now let's look at how aviation history has evolved. Only Static Strength was performed until 1900's. In 1940's was added Safe Life approach and was changed to Fail-Safety in 1955 after Comet catastrophe.

1.1. Comet catastrophe

Figure 1.1.1 Part of airplane

The de Havilland Comet 1 Aircraft aircraft experienced a series of breakdowns in flight before it was discovered that the fatigue life of the fuselage was much shorter than the tests showed.

British Overseas Airways Corporation (BOAC) Flight 783, de Havilland DH-106 Comet 1, G-ALYV

Near Calcutta, India, May 2, 1953 Flight 783 BOAC departed from Calcutta, India, on a flight to Delhi due to heavy rain and thunderstorm with 43 passengers and crew. Six minutes after takeoff, rising to 7,500 feet, the plane crashed in flight and crashed, killing everyone on board. Investigators concluded that the design of the aircraft failed due to overvoltage caused by strong gusts of the storm, or due to the pilot's excessive control of the aircraft when trying to fly through the storm. This was the first of three accidents that occurred during the destruction of the Comet aircraft structure.

Near Elba, Italy, January 10, 1954, Flight 781 BOAC flew from Rome, Italy, with a flight to London, England. Rising 27,000 feet, the plane suddenly crashed in flight and crashed into the Mediterranean Sea near the island of Elba. All 35 passengers and crew

on board were killed. After this accident, the Comet fleet was decommissioned and subjected to numerous modifications in areas considered to be the cause of an unknown malfunction. The fleet was returned to service at the end of March 1954.

An investigation conducted during a thorough study of the Elba fragments showed that the relatively square windows created stress concentrations that were significantly higher than expected. These stress concentrations tired the material around the corners of the window, which would quickly lead to a rupture of the fuselage.

On May 2, 1953, one year to the day after the maiden flight of the British-made de Havilland Comet, aircraft G-ALYV departed Calcutta Airport for Delhi as BOAC Flight 783. A few miles out of the airport, the flight encountered a severe thunderstorm. While the pilot and air traffic control were both aware of it, the storm did not appear severe enough to restrict flight through it. Furthermore, the captain was well-qualified, had considerable experience on this route, and had experience in similar weather conditions. Just six minutes after take off, while climbing to 7,500 feet, radio communication was lost. About this same time, witnesses at various ground locations saw "an aircraft coming down in a blaze of fire through severe thunderstorm and rain" and then crash into the ground. All 37 passengers and six crew members were killed.

The inquiry into the accident, directed by the Central Government of India, concluded that the crash near Calcutta was due to "structural failure of the airframe during flight through a thundersquall." They determined that one of two possibilities caused an overstressing of the plane enough to crash it: either severe gusts from the storm, or over-controlling by the pilot because of the storm. They recommended that the wreckage be more thoroughly analyzed to determine the primary failure, and that "consideration should be given" to modifying the flying characteristics of the Comet to give it more "feel" when loads are applied to the control surfaces.

Figure 1.1.2 Comet G-ALYP at Calcutta/Dum Dum

Copyright Matthew Clarkson - Used with permission

On January 10, 1954, Comet G-ALYP departed Ciampino Airport, Rome for London as BOAC Flight 781. About 20 minutes into the flight, as it was approaching 27,000 feet, transmission from the crew ceased mid-sentence, indicating a failure of the aircraft with "catastrophic suddenness." Witnesses on the island of Elba, Italy, saw the aircraft fall into the sea in flames. All 29 passengers and six crew members were killed.

While a crash investigation is normally conducted by the government or aviation authority in the country of the crash, it was determined that the British authorities would head the Elba investigation. The Comet fleet was grounded while investigation began and while de Havilland made modifications "to cover every possibility that imagination has suggested as a likely cause of the disaster." These modifications were made to address any possible cause of failure including flutter of control surfaces, primary structural failure due to gusts, flying controls, explosive decompression, engine fire, failure of a turbine blade, and fatigue of the wing. Fatigue of the fuselage was not considered as a cause at this time, nor was a modification made to compensate for it.

As these modifications were made, and while wreckage was still being recovered, the British Minister of Transport and Civil Aviation noted "the nature and extent of the modifications planned... and whilst the Calcutta disaster is completely accounted for... we cannot eliminate that the accident might have been due to some other cause which

was possibly common to both disasters." Believing the unknown cause of possibly two accidents had been fixed during the massive modification project, Comet flight was resumed March 23, 1954.

Just over two weeks later, on April 8, 1954, Comet G-ALYY departed Ciampino Airport, Rome for Cairo, as South African Airlines Flight 201, chartered through BOAC. About 40 minutes into the flight, while climbing through 35,000 feet, the aircraft experienced a catastrophic in-flight break-up and crashed into the sea near Naples. All 14 passengers and seven crew members were killed.

Immediately following this crash, BOAC suspended all Comet flights. The Airworthiness Certificate was removed from all Comet aircraft and the fleet was subsequently grounded indefinitely. It would take four years for the Comet to conduct commercial airline flights again - this time as the Comet 4.

Very minimal wreckage of the Naples aircraft was able to be recovered due to the great depth to which it had sunk - about 3,300 feet. From what was able to be recovered, it was concluded that there were no inconsistencies with "the view that the accident to Yoke Yoke [Naples] was attributable to the same cause as the accident to Yoke Peter [Elba]."

Fuselage Testing. With still no definitive cause, investigators decided to do full-scale tests on existing fuselages: unpressurized flight tests on G-ANAV and pressure tests on G-ALYU. To conduct the pressure tests in a safer manner, a water tank was constructed to encase the fuselage. The fuselage was submerged and filled with water, and then additional water was pumped into the cabin until the pressure inside the fuselage reached 1P, the equivalent of flight. This was then cycled to simulate many flights over the life of an aircraft. By using water instead of air, water being a much less compressible fluid, the test would be much safer and the fuselage would be able to be

repaired and re-tested as necessary. Had air been used, the results would have resembled the catastrophic in-flight break-ups at Elba and Naples.
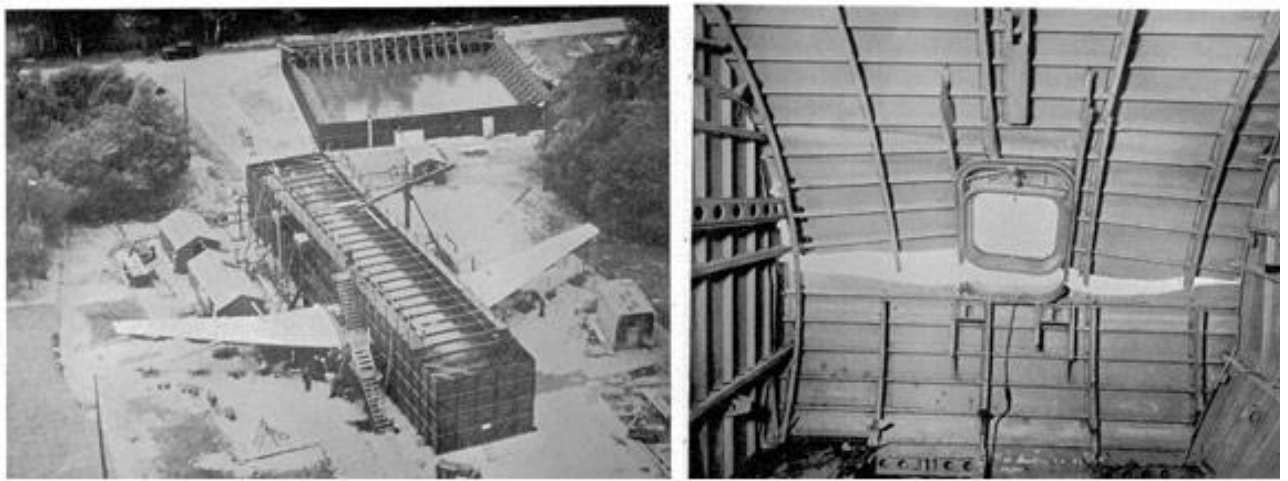

Figure 1.1.3 Comet G-ALYU in the water tank for pressure tests. The fuselage failed at a corner of e squarish forward escape hatch window.

G-ALYU had undergone 1,230 pressurized flights before testing and 1,830 tank "flights" before the fuselage failed at the corner of a squarish forward escape hatch window. This failure was the pivotal evidence needed to turn the direction of the investigation towards fatigue. A scale model was next created to test the theory of fatigue failure of the fuselage at a window corner. The results were then mapped to the crash site near Elba, and a new search area created. At this new location, the aircraft's Automatic Direction Finder (ADF) windows, also squarish, were recovered within hours. The ADF windows are on the very top of the fuselage, just forward of the wings. This piece of Elba wreckage, containing the two ADF windows and adjacent material bore the "unmistakable fingerprint of fatigue," and was determined to be the first fracture of the Elba crash.

G-ALYU withstood about 3,060 pressurized "flights," whether in the air or in the water tank. The Elba aircraft had experienced 1,290 pressurized flights. The Naples

aircraft made 900 pressurized flights. All these seemed to indicate a much lower fatigue life than the 16,000 successful cycles de Havilland tested.

Even in the design stage, de Havilland knew that the Comet would be a great technological advancement. They were competing to be the first company to offer pressurized jet service to the public. Since there was little experience in the design and production of pressurized commercial airliners at the time of the Comet development, deHavilland placed special emphasis on structural testing. One area of special emphasis involved pressure testing of the fuselage at higher than normal pressures.

Both the International Civil Aviation Organization (ICAO) and the British Civil Aircraft Requirements (BCARs), the applicable regulations for any British-made civil aircraft of the day, required a design pressure of 2P and a proof test of the fuselage up to 1.33P, where "P" is the working pressure difference, or the pressure expected in normal flight. For the Comet, P was approximately 8.25 pounds per square inch (lbs/in2 or psi). Neither ICAO nor the British authorities were fully aware of all the implications and effects of pressurized flight yet, so many regulations remained the same for pressurized and unpressurized aircraft, including the fatigue requirements.

De Havilland significantly exceeded the requirements in their effort to ensure the safety of their aircraft. They decided to design the fuselage to withstand up to 2.5P, and to proof test it to 2P, instead of just 1.33P. A prototype fuselage was pressurized between 1P and 2P approximately 30 times, and then pressurized to "rather over P" another 2,000 times. These two tests were to prove the fuselage as an adequate pressure vessel as well as to prove its structural integrity. Much later, in the summer of 1953 after Comets were already flying, regulations started to be published that required further fatigue testing for pressurized fuselages. Consequently, de Havilland went back and tested the same prototype fuselage with another 16,000 pressurization cycles between zero and 1P to verify its fatigue life. The fuselage finally failed at 16,000 cycles due to fatigue cracks

at the corner of a squarish cabin window. The Comet's expected life was only 10,000 cycles, so cracks at 16,000 were not a concern.

Stress Concentrations at Window Corners. De Havilland ran many tests in pre-production to prove the safety of the Comet: from pressure tests, to flight tests, to stress tests. The extensive proof testing of the fuselage was believed to be hard evidence that the Comet was safe. This experiential knowledge gained from actual testing bolstered de Havilland's confidence in their analyses. Calculations had been made for an average stress "in the neighborhood of the corners" which found the stress to be less than half the ultimate strength of the material. De Havilland did not consider further stress calculations to be any more accurate than the one already done, and preferred to rely on testing as the main evidence for the adequacy of the Comet. Following the failure of G-ALYU in the water tank however, more testing revealed stress at the window to be significantly higher than that originally determined. The testing found high stress concentrations at the window corners.

A stress concentration is a very localized area of much higher stress than the surrounding area. The stress concentrations were high specifically because of the squarish shape of the windows and window frames which is very different from the round/oval shapes of modern airplane windows. With modern windows, the stress flows freely around the curved edges with minimal build up. But with the Comets' squarish windows, stress cannot smoothly flow around the abrupt corners. This creates stress concentrations.

Although any aircraft will have varying levels of stress concentrations, the Comet's unique squarish window corners resulted in especially high stress levels. De Havilland tested their prototype to 2P, twice the expected operating pressure. The pressure overload combined with the very high stress levels at the window corners, created stress levels at the concentrations great enough to change the material

characteristics at these locations. Each time de Havilland increased the pressure load, the material characteristics progressively changed. Upon achieving the highest load of 2P, these locations had fundamentally different material characteristics than a production Comet. The process by which the material characteristics changed is called cold-working.

Material Cold-Work Properties. Cold-working is not, in itself, a safety issue. The testing to 2P proved the Comet could withstand excessive pressure loads. The significant misstep was the decision to perform the fatigue test on the same prototype fuselage that had undergone the pressure test and had been cold-worked. The prototype fuselage withstood 16,000 cycles before failure, due in large part to the fundamentally different material characteristics of the cold-worked material at the window corners. This characteristic change actually improved the fatigue properties at these locations, which would mask the true fatigue vulnerability of the production Comet. An animation describing how the material characteristics can be changed through cold-working is available at the following link

The Comets that crashed at Calcutta, Elba, and Naples, and G-ALYU in the water tank, had not undergone proving tests to 2P, nor had any other production Comet. These airframes did not have the "benefit" of the application of high loads to improve their fatigue characteristics. As a result, the window corners' natural cycles of stress would quickly wear out, or fatigue, the material. The fatigue had such a great effect on the never-overloaded production fuselages that instead of 16,000 cycles of fatigue life, the Comets were only reaching about 1,000 cycles. At the end of their fatigue lives, the worn-out material would rupture catastrophically, resulting in inflight breakup.
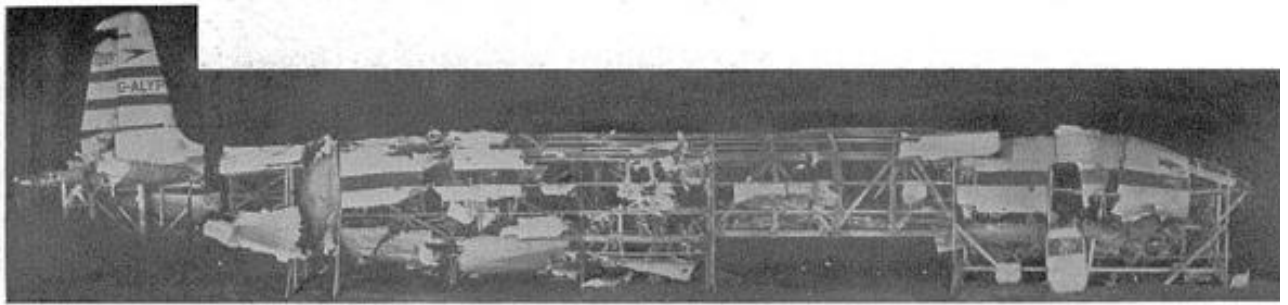
Figure 1.1.4 Reconstruction of the Elba fuselage wreckage recovered.

And Fatigue Analysis Methods introduced (60's – 70's)

The history of aviation development continued not without errors, so it was added Damage Tolerance in 1978 after Dan-Air catastrophe

1.2. Dan-Air catastrophe

In Zambia, Africa, on May 14, 1977, a Boeing Model 707-300 aircraft operated by Dan-Air, Ltd crashed while landing in Zambia, Africa. The accident occurred in daylight and in fine weather. The horizontal stabilizer of the aircraft was found 200 meters from the wreckage, which indicated the separation of the structure during the flight. A study of a broken stabilizer showed that the fail-safe design characteristics did not work properly. Further studies showed that structural changes designed to statically strengthen the stabilizer structure, as part of the 707-300 design, also caused higher than expected fatigue loads and subsequent failure of the stabilizer structure.

The third flight of the day for the Dan-Air aircraft proceeded normally and without incident, until final approach at Lusaka.

The flight data recorder provided the following details:

- At 09:07 hours the co-pilot contacted Lusaka Approach, and at 0911 the aircraft was cleared to descend to Flight Level (FL) 110 (11,000 feet altitude).
- At 09:23 hours the co-pilot reported that the aircraft was leveling at FL 110 at a Distance Measuring Equipment (DME) range of 37 nautical miles from Lusaka.

- At 09:28 hours the co-pilot reported that the airfield was in sight.

- At 09:29 the co-pilot reported that the airplane was turning downwind.

- At 09:32:02 the Lusaka Approach controller gave the aircraft a clearance to make a visual approach to runway 10. The co-pilot replied "Roger." This was the last transmission received from the aircraft.

- At 09:32:53 hours the readout from the cockpit voice recorder (CVR) indicated that 50-degree flaps had been selected.

- At 09:33:11 the landing checks had been competed.

Six seconds later, 24 seconds after selection of landing flaps, at 0933:17 hours, a loud "break up" noise was recorded with the CVR record terminating five seconds later, at 0933:22 hours.
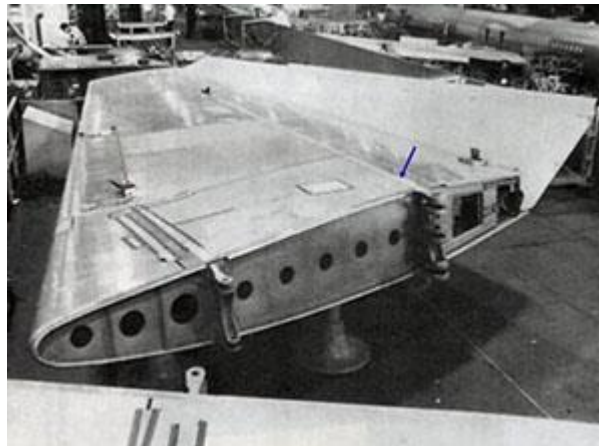
Figure 1.2.1 Photo of right hand stabilizer in jig, showing clevis attachments at the front and rear spars.Photo taken from accident report

Eyewitnesses on the ground observed the Dan-Air flight on what appeared to be a normal approach to runway 10 at Lusaka International Airport. They saw a large piece of the aircraft structure separate in flight. The aircraft pitched rapidly nose down and dived vertically into the ground from a height of about 800 feet, approximately two miles short of the runway threshold, and caught fire upon impact. The accident occurred in daylight and in good weather. All 6 occupants of the aircraft were killed.

The complete right side horizontal stabilizer and elevator assembly were found 200 meters back from the airplane wreckage site, indicating the separation occurred in flight prior to the aircraft pitching nose down into its final dive. The cause of the stabilizer separation became the focus of the investigation.

Horizontal Stabilizer Structure.The horizontal stabilizer is a box structure, with the forward and aft sides of the box being the front spar and rear spar, respectively. The top and bottom surfaces of the stabilizer box are formed by skin structure. The stabilizer is attached to the fuselage by lug and clevis attachments at the front and rear spars. The center of lift of the horizontal stabilizer is located slightly aft, such that the normal load distribution is split between the front spar and rear spar at approximately 5% and 95%, respectively.

Aerodynamic Affect of Horizontal Stabilizer Failure

The diagram below shows the relative locations of aircraft center of gravity, center of lift, and balancing tail load of a typical transport category aircraft in flight:

- The design of transport category aircraft results in a natural tendency to pitch the airplane nose down
- Balance (longitudinal stability) is provided by the downward acting force of the horizontal stabilizer
- Loss of the horizontal stabilizer results in an unbalanced nose-down pitch and loss of control
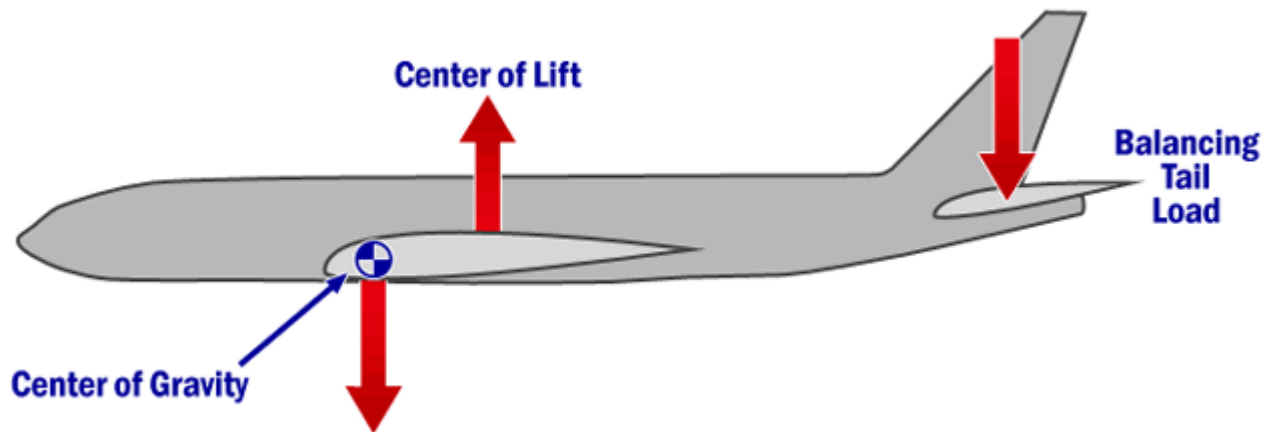
Figure 1.2.2 Diagram of locations of center gravity, center of lift, and balancing load
of aircraft
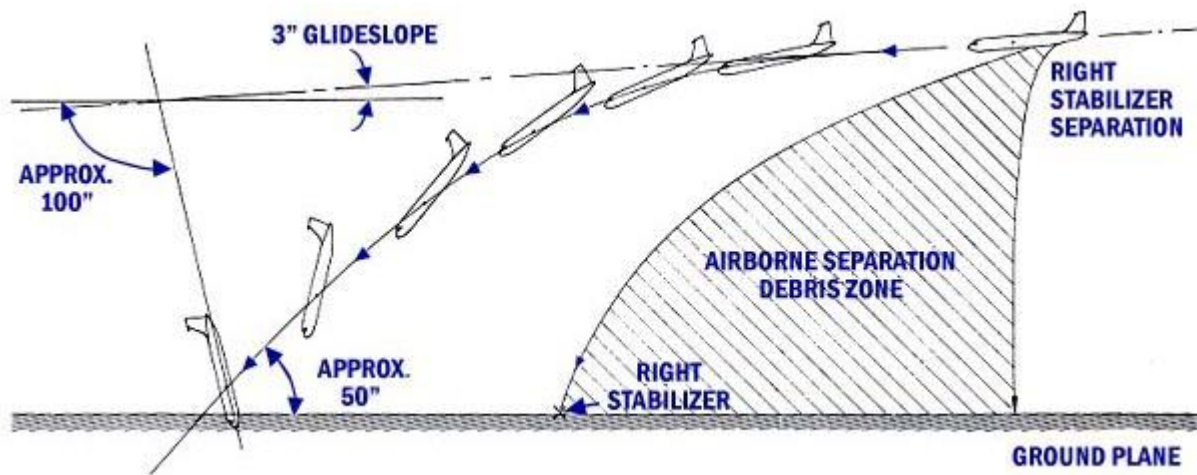
Figure 1.2.3 Diagram of Dan-Air accident, taken from accident report

Examination of the detached stabilizer revealed evidence of a fatigue failure of the top
chord of the rear spar, initiating at the 11th fastener hole, which is used by both the rear
spar upper chord and upper skin structure. The location of the fastener was 14.25 inches
outboard of the attachment of the stabilizer attachment pin.
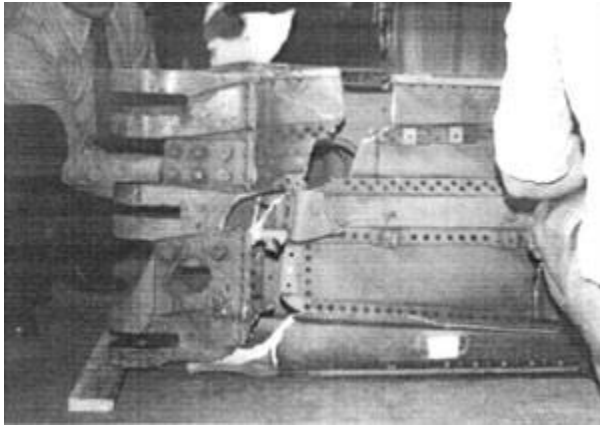
Figure 1.2.4 Photo of separation of Dan-Air right side stabilizer.
Accident investigation photo.
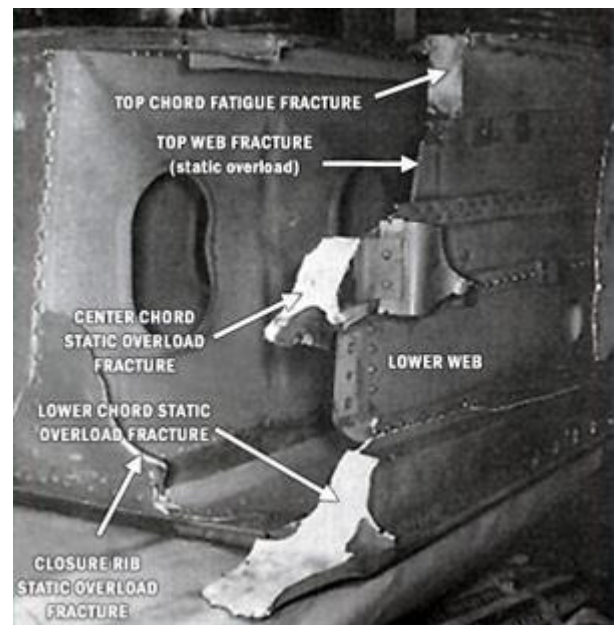
Figure 1.2.5 Photo of fracture face of Dan-Air accident aircraft right side horizontal stabilizer.
Photo taken from accident report.

The cracking progressed in fatigue over approximately 60% of the chord, and then began a series of several tensile jumps, separated by small periods of fatigue. The total number of flights between the initiation of the fatigue crack and the final failure of the upper chord was estimated by the investigators to have been approximately 7,200 flights, with 3,500 of the flights being the duration to grow the crack across the exposed surface of the top chord.

Failure of the top chord was followed by fracture of the upper web, center chord, lower web and lower chord, leading to loss of the stabilizer and loss of control of the aircraft.

The investigation discovered no unique feature leading to the cracking at the 11th fastener hole other than high stresses existing in the entire inboard area of the rear spar. The location of the 11th fastener hole is indicated by an arrow in the photo below.
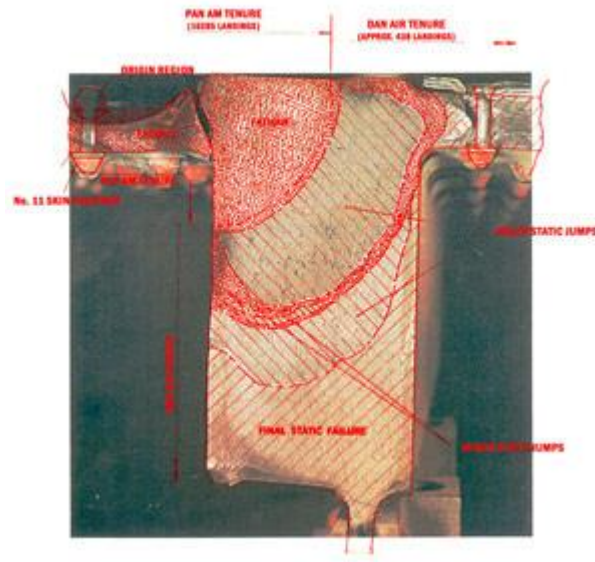
Figure 1.2.6 Photo of top chord fracture face, with crack progression identified.
Photo taken from accident report.

Post-accident inspection of the 707-300 in-service fleet discovered cracking occurring in the rear spar upper chord at the 11th fastener in three other aircraft. Cracks were also found in other fastener holes on either side of fastener hole 11, from holes 2 to 21. In total, cracks were found in 7% of the in-service fleet, equal to 38 of the 521 model 707-300s in operation.
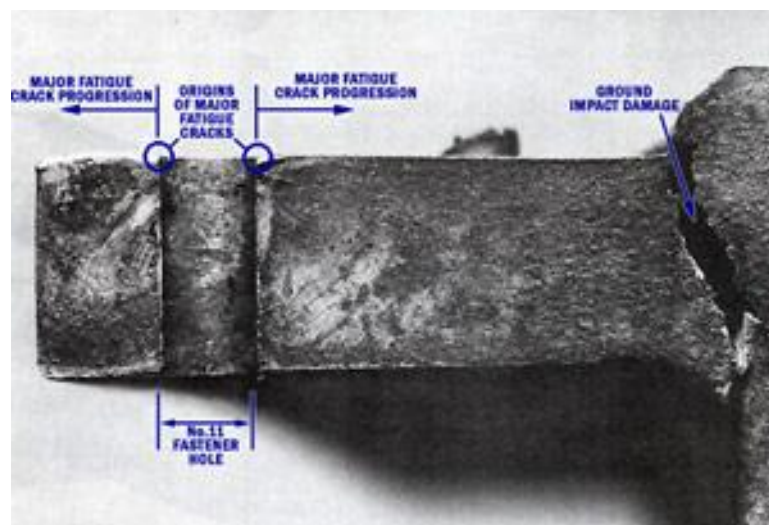

Figure 1.2.7 Photo of fracture face emanating from the 11th fastener
Photo from accident report.
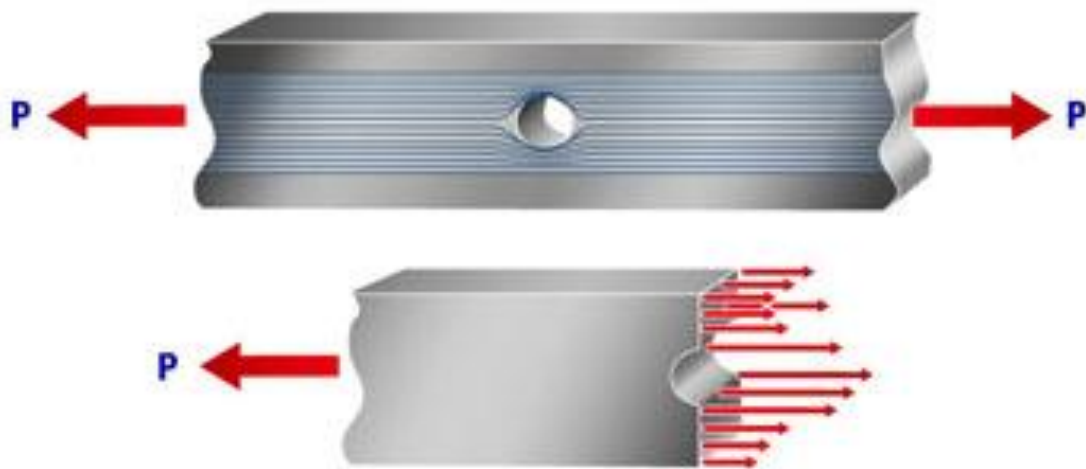
Figure 1.2.8 Diagram of stress concentration

Effect of a Fastener Hole in a Tensile Member: "Stress Concentration"

The top chord of the stabilizer rear spar is loaded in tension. A structural member of uniform cross section will have a uniformly distributed tensile stress across the section.

A structural member having a discontinuity, such as a fastener hole, will develop a stress field that is larger at the edges of the hole. This means that the stresses are higher at the edges of the hole than in the area away from the hole. This phenomenon is called a "stress concentration," and explains one of the causes of cracking typically found to occur at the location of the discontinuity.

Development of the Design of the 707-300 Stabilizer. The Dan-Air aircraft involved in this accident was the first model 707-300 produced by The Boeing Company. The Boeing 707 began with the KC-135 military transport and includes the 707-100, -200, -300, and -400 series of aircraft. The horizontal stabilizer on the early models, the 707-100 and 200 derivatives, are identical and have rear spars of two-chord design.

In order to certify the aircraft, the manufacturer demonstrated that the two-chord design of the horizontal stabilizer was "fail-safe." That is, with a failure of any single structural element, the remaining intact structure could carry the loads anticipated in flight. In the case of the horizontal stabilizer, the failure assumed most likely, and most critical, was

the failure of a single lug. In the case of the early 707 two-chord stabilizer design, the Boeing Company demonstrated through a series of dynamic tests that the horizontal stabilizer rear spar upper chord could fail, and that the stabilizer loads were reacted safely by the stabilizer box and remaining chord attachment.

The fail-safe philosophy of the 707-100, supported by the testing performed on the 707-100 two-chord design, was extrapolated to support certification of the 707-300 horizontal stabilizer. However, there were design differences between the two models that made the early tests invalid for the later model.

When the model 707-300 was developed, the stabilizer assembly was extensively redesigned. The stabilizer span was enlarged to increase tail volume. To accommodate the resulting increase in loading on the larger tail, the intended fail-safe characteristic of the structure was achieved by the addition of a third chord, with a lug and clevis attachment point, located at mid-spar depth on the rear spar.
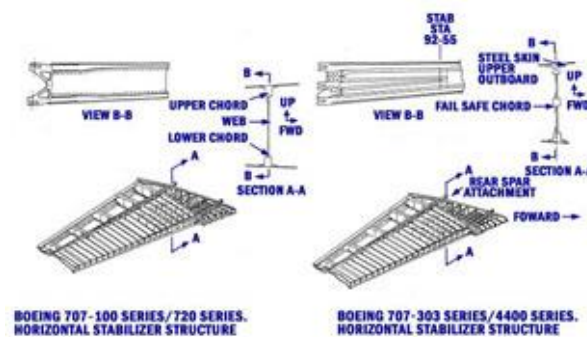
Figure 1.2.9 Diagram of horizontal stabilizer structure

(View Large Diagram)

The analysis performed on the new three-lug design of the 707-300 assumed the same failsafe scenario as was proven during testing of the two-lug stabilizer design of the 707-100/200: failure of the stabilizer rear spar upper lug. Testing was not performed to validate the failure scenario on the three-lug design because it was felt the 737-100/200 tests were representative.

For substantiation of the 707-300, Boeing used analysis to show that in the event of the upper lug failure the load would be redistributed to the lower two lugs, which would be able to carry the flight loads safely.

Another design change was made to the 707-300 as a result of a discovery made during the flight test program. Flight testing indicated that the 707-300 horizontal stabilizer lacked sufficient torsional stiffness. In order to correct this deficiency, the stabilizer lower aluminum skin was increased in thickness, and a stainless steel plate was used to replace a portion of the upper aluminum skin. The location of the stainless steel plate is shown as the shaded area on the figure below.
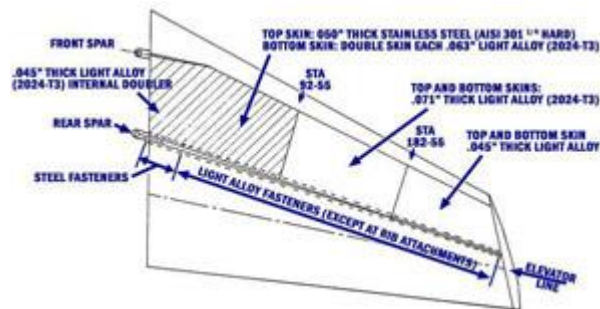
Figure 1.2.10 Diagram of the stabilizer lower aluminum skin thickness

View Large

The stainless steel plate was much stiffer than the aluminum structure to which it was attached. Without the plate, the aluminum horizontal stabilizer would deflect a certain amount under flight loading. With the stainless steel plate riveted to the stabilizer, the deflection was less because the steel plate resisted the bending. This bending resistance was transferred to the aluminum stabilizer rear spar through higher-than-expected loading in the fasteners.

The load increase on the stabilizer that occurred as a result of the stiffening of the skin panel led to the development of fatigue cracking in an area outboard of the lug. This

outboard location, which was not considered to be a likely failure scenario, was not analyzed by Boeing.

These two design changes in the 707-300 relative to the 707-100 (addition of the third chord and stainless steel plate) became significant factors leading to the loss of the Dan-Air aircraft.
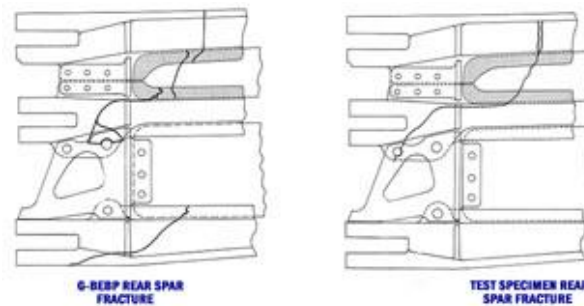
Post Crash Investigation

Figure 1.2.11 Diagram of rear spar fracture
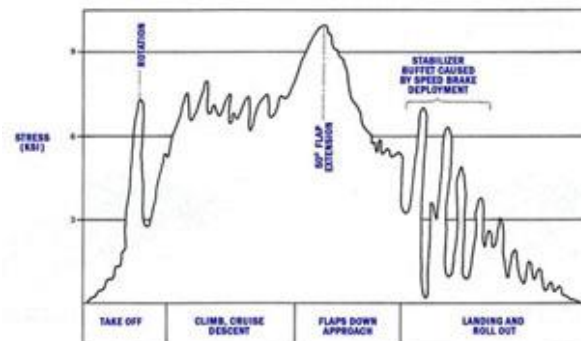
(View Large Diagram)

Figure 1.2.12 Diagram of the horizontal stabilizer load spectrum

(View Large Diagram)

Dan-Air 707-300, G-BEBP, Basic Aircraft Information:

- Investigation of the pilot and co-pilot revealed no anomalies.
- Aircraft: Manufactured - 1963

- Total airframe flight hours at time of accident - 47,621
- Total airframe flight cycles at time of accident - 16,723
- Flight hours since last C-check - 662
- Flight cycles since last C-check - 176
- Dan-Air G-BEBP was the first 707-300 produced by Boeing.

After the accident, a fail-safe test was performed on a 707-300 horizontal stabilizer. The top chord was cut to simulate the fatigue damage on the Dan-Air airplane. During testing, the spar fractured completely at a load approximating the load estimated to have been acting on the Dan-Air aircraft at the time of approach and stabilizer separation. Application of up elevator during approach was shown to produce loads 20% greater than the test failure load. This load discrepancy, and the strikingly similar fracture characteristics of the test specimen, indicated that the failure occurred as a result of an inability of the remaining structure to carry the flight loads subsequent to the fracture of the rear spar top chord.

Widespread Fatigue Damage approach was added in 1998 after Aloha catastrophe

1.3.   Aloha catastrophe

In Maui, HI on April 28, 1988, when flight 243 of Aloha Airlines leveled off at level 240 on an inter-island flight from Hilo to Honolulu, an 18-foot section of the upper fuselage suddenly left the plane, flipping the stewardess overboard. The captain made an emergency descent and headed for Maui, landing on the Maui 02 runway. Of the 95 people on board, there was one dead (stewardess) and eight serious injuries

The National Transportation Safety Council (NTSB) found that the likely cause of the accident was the failure of the Aloha Airlines maintenance program to detect significant disconnection and fatigue damage to the fuselage skin knees.

Limit of Validity and Damage Tolerance of Repairs was added to design philisophi in 2010.

2. A CRACK IN A STRUCTURE

2.1. STRESS AT THE CRACK TIP

In calculating the strength of structural elements and structures with cracks, the starting point is to study the distribution of stresses and strains that arise in them under the action of applied loads. Of particular interest is the region in the immediate vicinity of the crack tip, since the state P. occurs in it. Within the framework of linear fracture mechanics, which proceeds from the model of a perfectly elastic body and represents a crack as a section of zero thickness, whose surfaces are free of stresses, the problem under consideration reduces to boundary value problem of the theory of elasticity

I - Opening mode   II - Sliding mode   III - Tearing mode
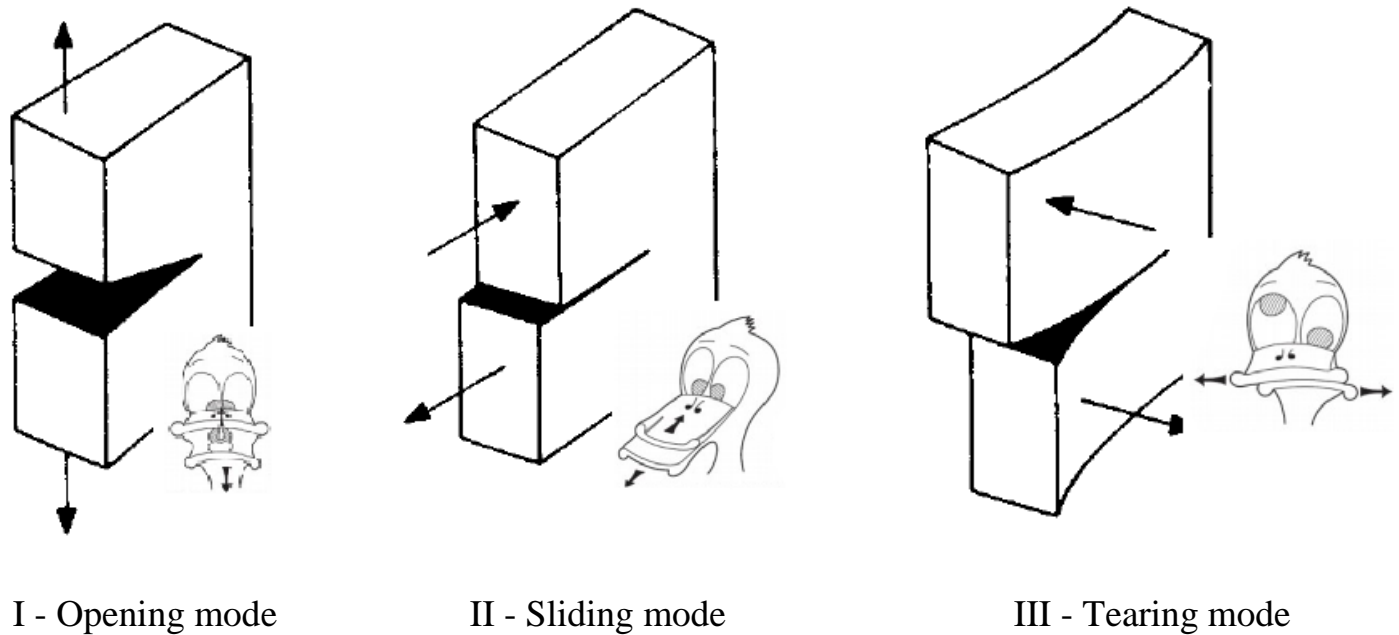
Fig. 2.1.1 The three modes of cracking

In the most general case, the distribution of deformations in the vicinity of an arbitrary point of the crack contour can be represented as a superposition of three particular types of deformation (Fig. 2.1.1), corresponding to the three main types of displacement of the crack surfaces: normal detachment (I), transverse (II), and longitudinal (Iii) shifts. The first type is associated with the normal displacement of the crack surfaces in mutually opposite directions; the second corresponds to displacements

in which the surface of the crack glides along each other in the direction perpendicular to its front (z axis).

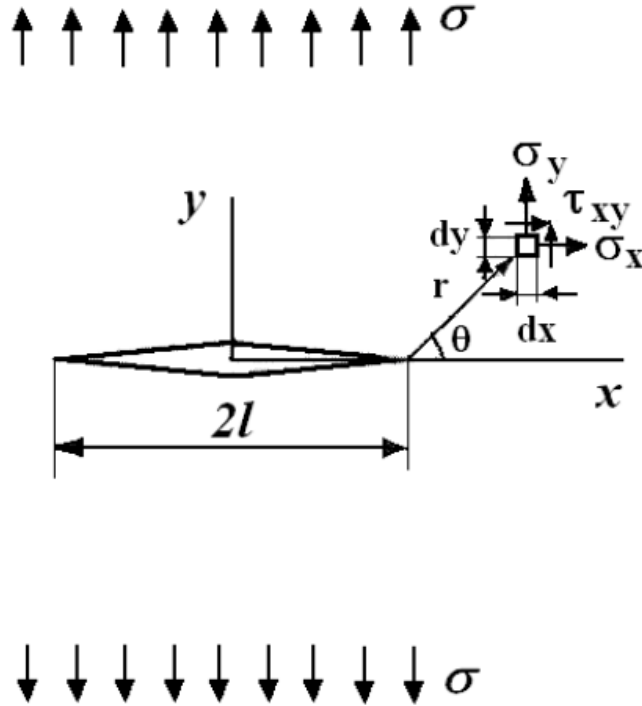Consider a through crack of type I with a length of 2l in an infinite plate, as shown in Fig. 2.1.2

Fig. 2.1.2 Endless plate crack

The plate is under the action of tensile stress σ, which is caused by forces applied at infinity. The *dxdy* element of the plate, located at a distance *r* from the crack tip and making an angle θ with the plane of the crack, is affected by normal stresses σ_x and σ_y, acting in the x and y directions and tangential stress τ_{xy}. It can be shown that these stresses are equal:

$$\sigma_x = \sigma\sqrt{\frac{l}{2r}}\cos\frac{\theta}{2}\left(1 - \sin\frac{\theta}{2}\sin\frac{3\theta}{2}\right); \qquad \tau_{xy} = \sigma\sqrt{\frac{l}{2r}}\sin\frac{\theta}{2}\cos\frac{\theta}{2}\cos\frac{3\theta}{2};$$

$$\sigma_y = \sigma\sqrt{\frac{l}{2r}}\cos\frac{\theta}{2}\left(1 + \sin\frac{\theta}{2}\sin\frac{3\theta}{2}\right); \qquad \sigma_z = v\,(\sigma_x + \sigma_y)$$

$$(2.1.1)$$

In the elastic case, the stresses indicated in (2.1.1) are proportional to the external stress σ. Their values are proportional to the square root of the crack size and tend to infinity at the crack tip when r vanishes. The dependence of σ_y on r for θ = 0 is shown in Fig. 2.1.3.
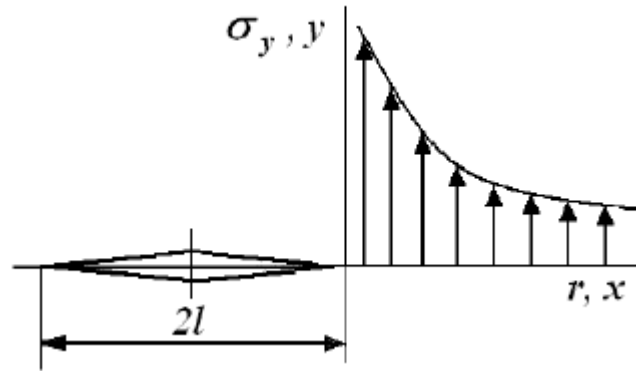

Fig. 2.1.2 Elastic stress σ_y at the crack tip.

For large values of r, the quantity σ_y tends to zero, while it should tend to σ. Obviously, equations (2.1.1) are valid only in a limited region - near the crack tip. Each of the equations is the first member of the series.

In the vicinity of the crack tip, these first terms describe the stress fields quite accurately, since the other terms are small compared to them. At large distances from the crack tip, a larger number of terms should be introduced into the equations.

In equations (2.1.1), the coordinate functions r and θ have a simple form. In a generalized form, these equations can be written as follows:

$$\sigma_u = \frac{K_I}{\sqrt{2\pi r}} f_u(\theta), \text{ where } K_I = \sigma\sqrt{\pi l} \tag{2.1.2}$$

The K_I coefficient is called the stress intensity factor (SIF), where the index I denotes the type of failure I. When the SIF is known, the stress field at the crack tip is completely defined.

Equations (2.1.1) can be modified to fit equations(2.1.2):

$$\sigma_x = \frac{K_I}{\sqrt{2\pi r}}\cos\frac{\theta}{2}\left(1 - \sin\frac{\theta}{2}\sin\frac{3\theta}{2}\right); \qquad \tau_{xy} = \frac{K_I}{\sqrt{2\pi r}}\sin\frac{\theta}{2}\cos\frac{\theta}{2}\cos\frac{3\theta}{2};$$

$$\sigma_y = \frac{K_I}{\sqrt{2\pi r}}\cos\frac{\theta}{2}\left(1 + \sin\frac{\theta}{2}\sin\frac{3\theta}{2}\right); \qquad \sigma_z = v\,(\sigma_x + \sigma_y); \qquad (2.1.3)$$

Thus, the stress field is determined by the stress intensity factor. This factor also determines what happens inside the ductility zone. K_I is a measure of all stresses and strains. When stresses and strains at the crack tip reach critical values, the crack expands. Power criterion J.R. Irvina beginning crack growth has the form:

$$K = Kc \qquad (2.1.4)$$

This means that when KI reaches a critical KIC value, destruction will occur. It can be assumed that KIC is a material constant, a critical value of the stress intensity factor at the time of failure:

$$K_{IC} = \sigma_c\sqrt{\pi l} \qquad (2.1.5)$$

Expression (2.1.5) for the stress intensity factor is valid only for an infinite plate. For a plate of finite dimensions, this formula takes the form:

$$K_I = \sigma\sqrt{\pi l} \cdot f\left(\frac{l}{W}\right)$$

where W is the width of the plate. To determine the KIC, it is necessary to know the function f (1 / W). Of course, f (1 / W) tends to unity for small values of l / W. The true KIC value can be obtained empirically only if the displacements of the plate points perpendicular to its plane are sufficiently small, i.e., when the plate has a sufficient thickness. In the case of flat stress, the critical SIN value will depend on the thickness of the plate. Stress intensity factors are usually presented as

$$K = \sigma\sqrt{\pi l}Y \qquad (2.1.7)$$

This equation (2.1.7) is the Griffith criterion and I will use it in my work.

2.2.   STRESS INTENSITY FACTOR

The calculation of the body on the durability is inextricably linked with the determination of its stress-strain state. This is necessary not only for the purpose of inspection of dangerous points, but also for vessels for simple materials, which are based on different criteria of the following dangerous states. For many other bodies, the determination of the stress-strain state at a dangerous point is intended to derive the coefficients that create, which are the ratio of the maximum value, which are either components subject to the corresponding nominal value and thus equalized by dimensionless numbers.

In the presence of a crack in the body to judge the nature of its possible spread and, accordingly, the strength of the body also requires knowledge of the ensely deformed state in the region of the crack tip. However, this problem differs from the usual problem of determining the coefficient of stress concentration in that the linearized formulation of boundary conditions and the physically linear theory of elasticity lead to infinite stresses near the vertex. In this case, the concept of the stress concentration coefficient is meaningless. The pattern of stress and strain distribution in the vicinity of the crack tip does not depend on the crack length, body shape, and the scheme of operating loads [2]. The intensity of this asymptotic distribution is determined only by the stress intensity factor (SIF) K, which does not depend on the coordinates of the points near the vertex. Therefore, the processes of material destruction occur and are determined by the intensity of the stress field surrounding the crack, and are characterized by SIF. In contrast to the concentration coefficient, the SIF is a dimension ($[K] = Pa \cdot m^{1/2}$]).

2.3.   GRIFFITH – OROWAN – IRWIN CONCEPT

It was originally believed that the theory of A.A. Griffiths is applicable only to fragile materials such as glass. Its use for other materials, such as, for example, metals, was hindered by the fact that their destruction is always accompanied by plastic deformations in the prefracture zone - in a more or less extensive neighborhood of the tip of the crack. Hungarian scientist E.O. Orovan, conducting experiments on plates of mild steel with cracking, clearly saw how such deformations occur. E.O. Orovan noted that plastic deformation is concentrated in a thin layer near the surface of the crack. This behavior has been called quasibrittle.

E.O. Orovan and J.R. Irwin proposed to take into account the plastic work in the framework of the same scheme A.A. Griffiths, assigning a broader meaning to surface energy and replace γ with the sum $(\gamma + \gamma_p)$, where γ_p is the work of plastic deformation during the formation of a surface unit.

Of course, due to the irreversibility of γ_p, now we can only speak of crack growth. It is important to emphasize that for metals $\gamma_p \gg \gamma$. For example, for steel $\gamma_P \approx 10^3 \gamma$. It is such significant plastic work that provides good resistance of metals to brittle fracture.

Now the formula is A.A. Griffiths (2.1.7) can be rewritten as:

$$\sigma = \sqrt{\frac{2E(\gamma + \gamma_P)}{\pi L}} \qquad (2.1.8)$$

It follows from (2.9) that, as before,

$$\sigma_C \sqrt{\pi l} = \sqrt{2E(\gamma + \gamma_P)} = \text{const} \qquad (2.1.9)$$

Thus, the concept of quasi-brittle fracture E.O. Orovan and J.R. Irvina was a major contribution to the mechanics of fracture and allowed me to switch from an ideal material to A.A. Griffiths to real metallic materials.

3. MODELING AND ANALYZIS

The calculation of the stress-strain state in the area of the top of the main crack in the fuselage skin of passenger plane is implemented in this section.

There is a plate of skin, typical open hole with crack. Plate is fabricated from Aluminum 2024 – T3, Clad Sheet. It has 0.063 inch thick and 3.375 inch in longitudinal direction (X axis) and 1.6875 inch in hoop direction(Y axis) figure 3.1 .
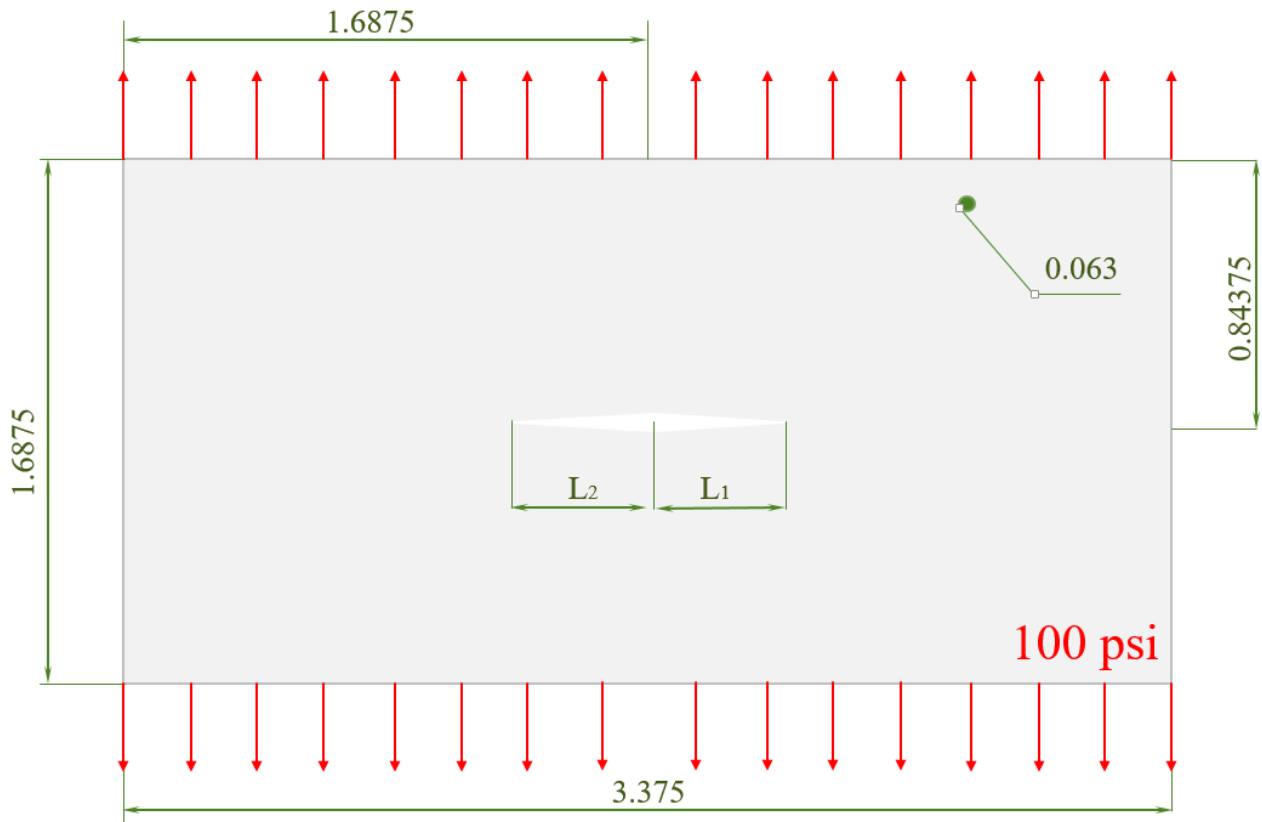

Fig. 3.1 Geometric parameters and Loads

An analysis of crack growth from 0.126 inches to 1.26 inches was performed and the characteristics of stress, stress intensity, and the dependence of stress intensity and geometric factor on crack length were obtained using the CosmosM software package.

Analysis has ten stages. Details for each stage are listed below.

COSMOS/M is a complete, modular, self-contained finite element system developed by Structural Research and Analysis Corporation (SRAC) for personal computers and workstations. The program includes modules to solve linear and nonlinear static and dynamic structural problems, in addition to problems of heat transfer, fluid mechanics, electromagnetics and optimization. Modules for such special analysis options as fatigue are also available. The system is constantly developed and maintained by using state-of-the-art techniques and up-to-date hardware capabilities.This chapter introduces the COSMOS/M product line and outlines the features of its various modules.
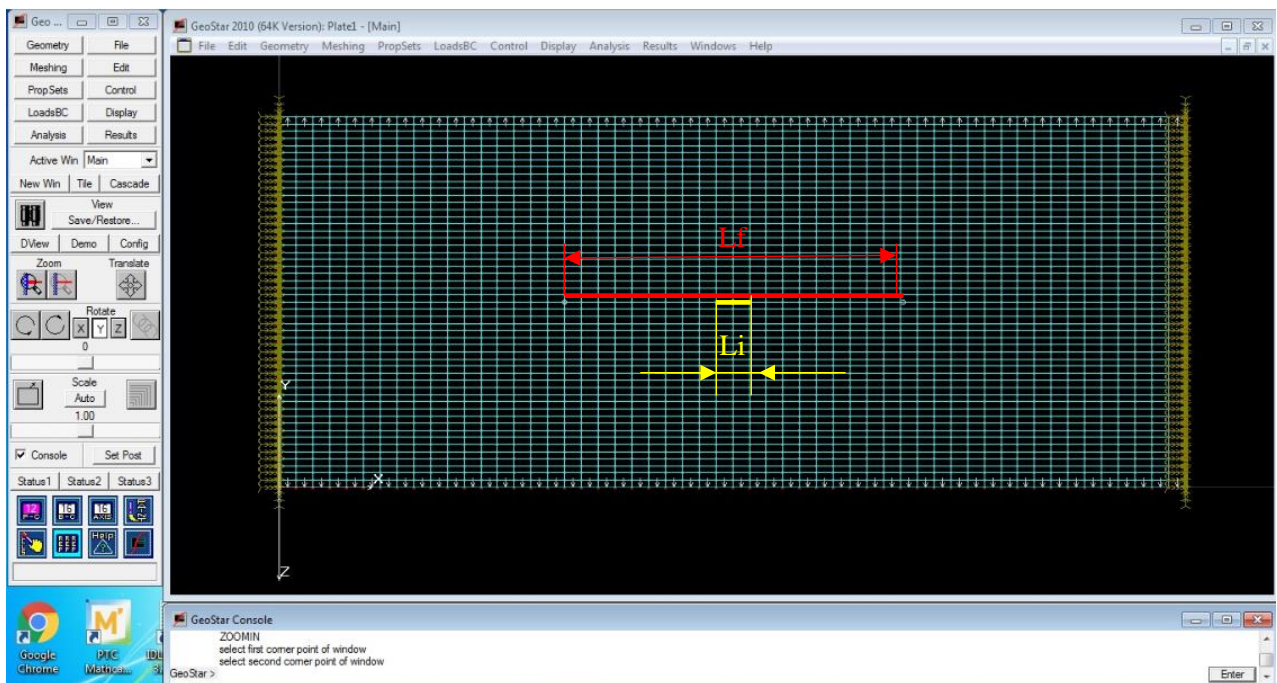
Fig. 3.2 FEM model in Cosmos\M

Crack grew from node number 1457 to 1448 and from 1459 to 1468. The results are the same for a both parts.

If Fsu/Ftu = 39/69 = 0.619 > 0.577 – using energy theory of stress [7].

The studied object (sample) is a rectangular plate of size a × b = 3.375 × 1.6875 inches with a single central transverse crack with a length of 2l = 0.126 inches. This specimen is stretched by a uniformly distributed force P = 100 psi perpendicular to the crack line (Fig. 3.1). The plate is made of an isotropic material with the following physico-mechanical characteristics: E = 1.05e7 psi, μ = 0.3, Ftu = 63000 psi. The sample thickness equal to 0.063 inches is much less than the rest of its overall dimensions, so we can conclude that the object is in a plane stress state.

In this approach, at each of the 10 stages of calculation, we set the material parameters and loading, which do not change throughout all 10 stages, and the length of the crack, the specific location of the crack, which will be determined for each stage separately.

This calculation method is universal for any aircraft design at the moment. At each of the 10 stages of crack growth, we obtain results in the form of normal stresses according to 4 strength theory and stress intensity factor. Further, in the process of data processing, we see the dependence of the coefficient of stress intensity on the length of the crack at each stage, respectively, we can build the dependence of the geometric coefficient of coefficients that takes into account the effect on the stress field of the lateral sides of the plate of finite width on the length of the crack.

For all stages:

• length of plate - a = 3.375 inches

• width of plate - b = 1.6875 inches

• Material: 2024-T3 Clad Sheet, t = 0.063 inch

• Young's modulus - E = 1.05e7 psi

• Poisson ratio - μ = 0.3

• Ultimate tensile strength - Ftu = 63000 psi
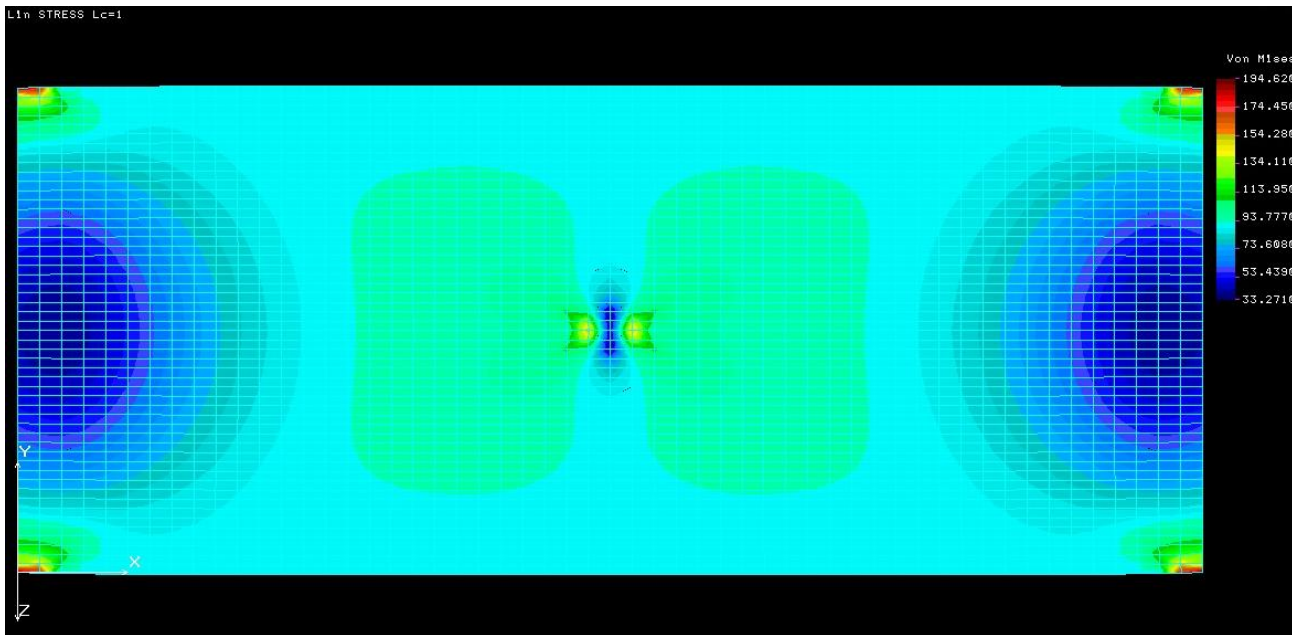
Stage 1

L = L1 + L2 = 0.063 + 0.063 = 0.126 inch

Fig. 3.3 Stress Von Mises in Stage 1
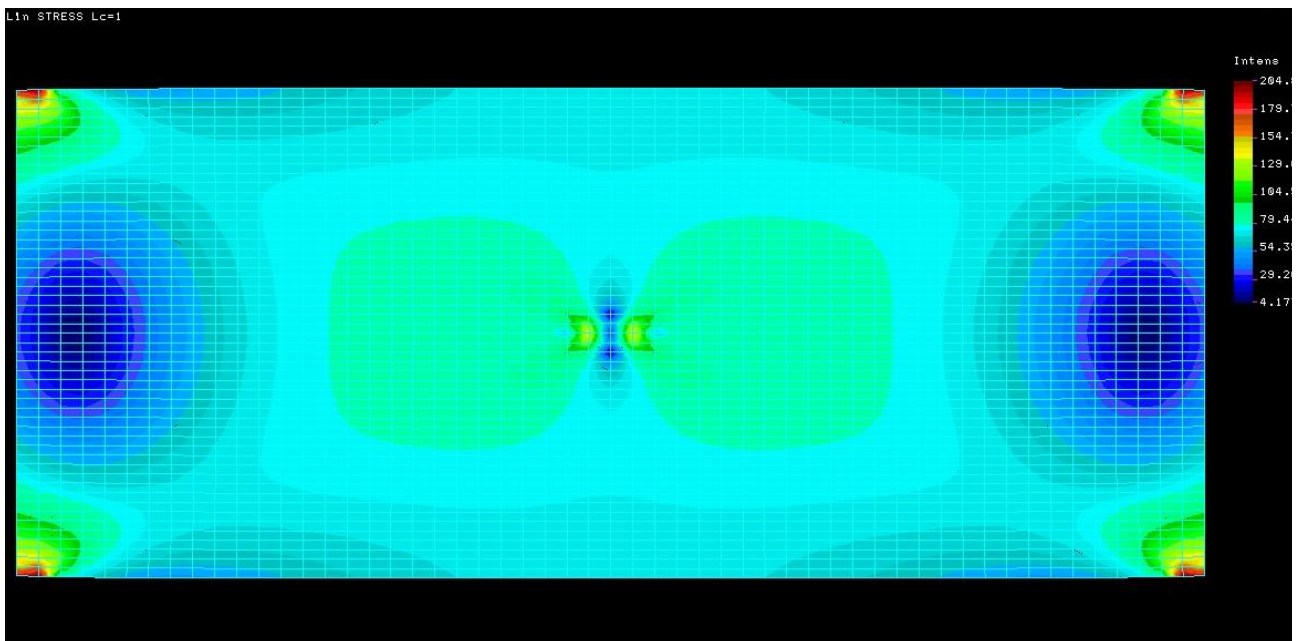

Fig. 3.4 Stress Intesity in Stage 1

Stage 2

L = L1 + L2 = 0.126 + 0.126 = 0.252 inch
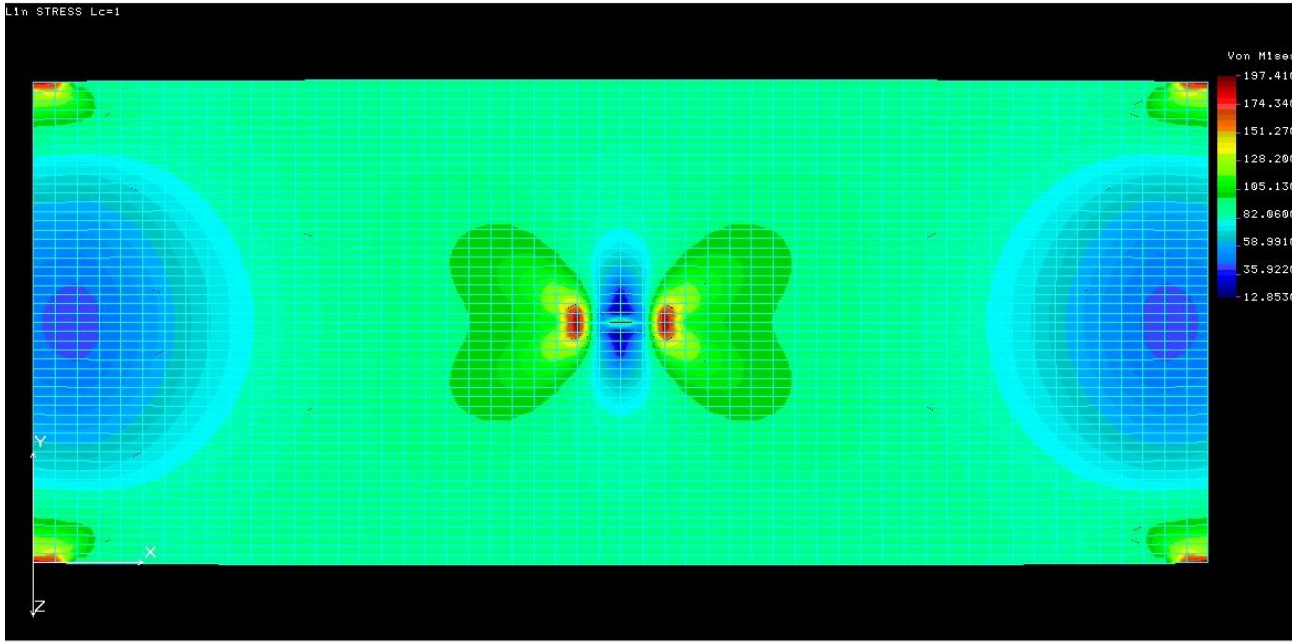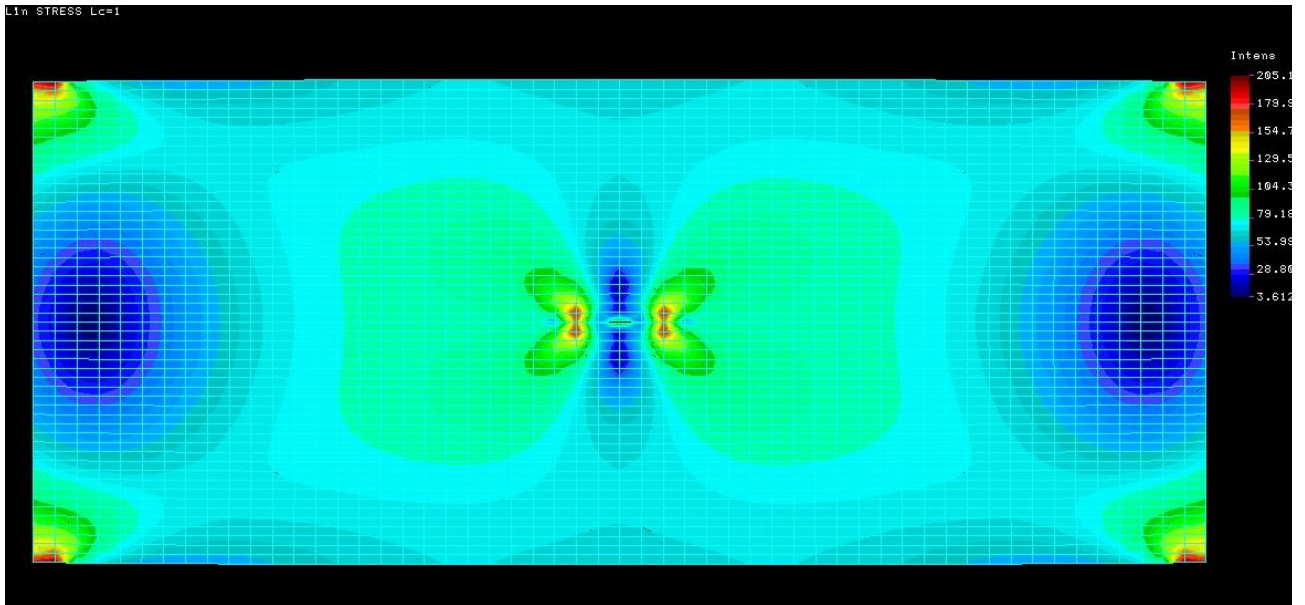

Fig. 3.5 Stress Von Mises in Stage 2

Fig. 3.6 Stress Intesity in Stage 2
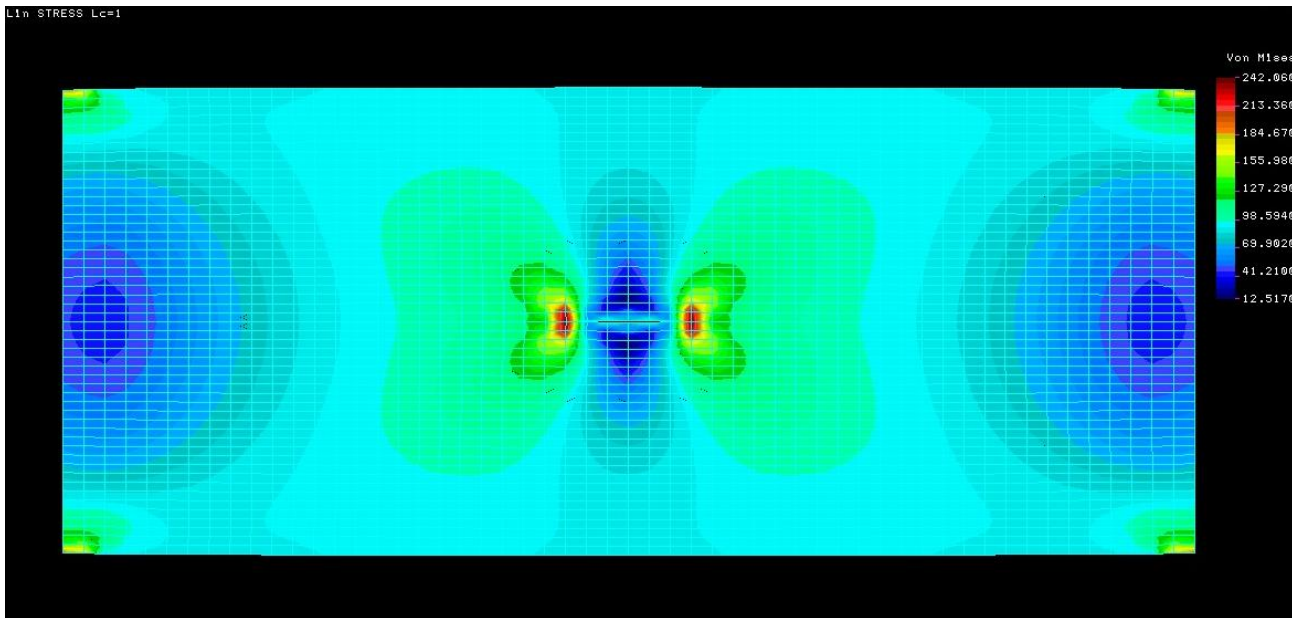
Stage 3

L = L1 + L2 = 0.189 + 0.189 = 0.378 inch
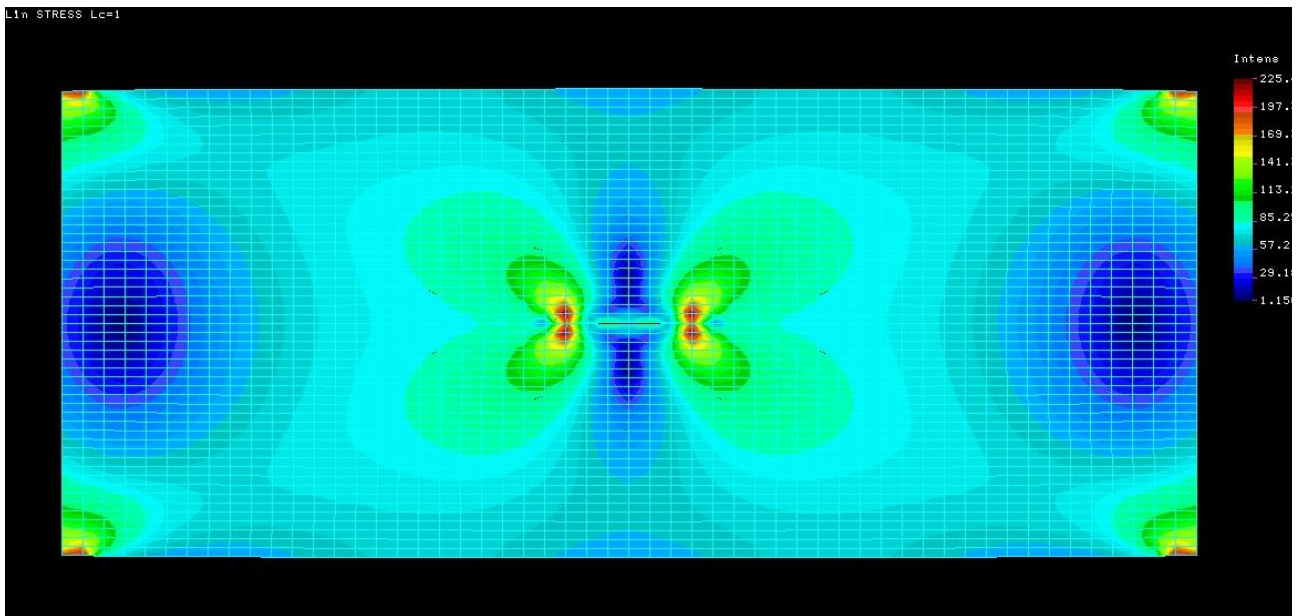

Fig. 3.7 Stress Von Mises in Stage 3

Fig. 3.8 Stress Intesity in Stage 3
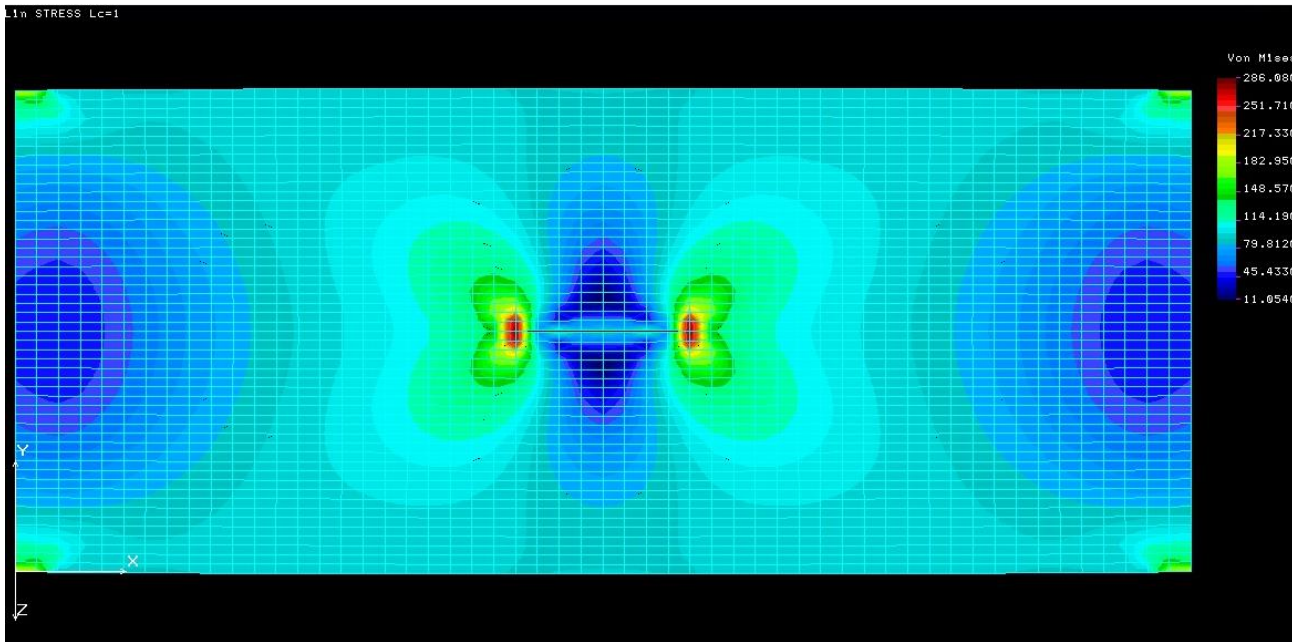
Stage 4

L = L1 + L2 = 0.252 + 0.252 = 0.504 inch

Fig. 3.9 Stress Von Mises in Stage 4
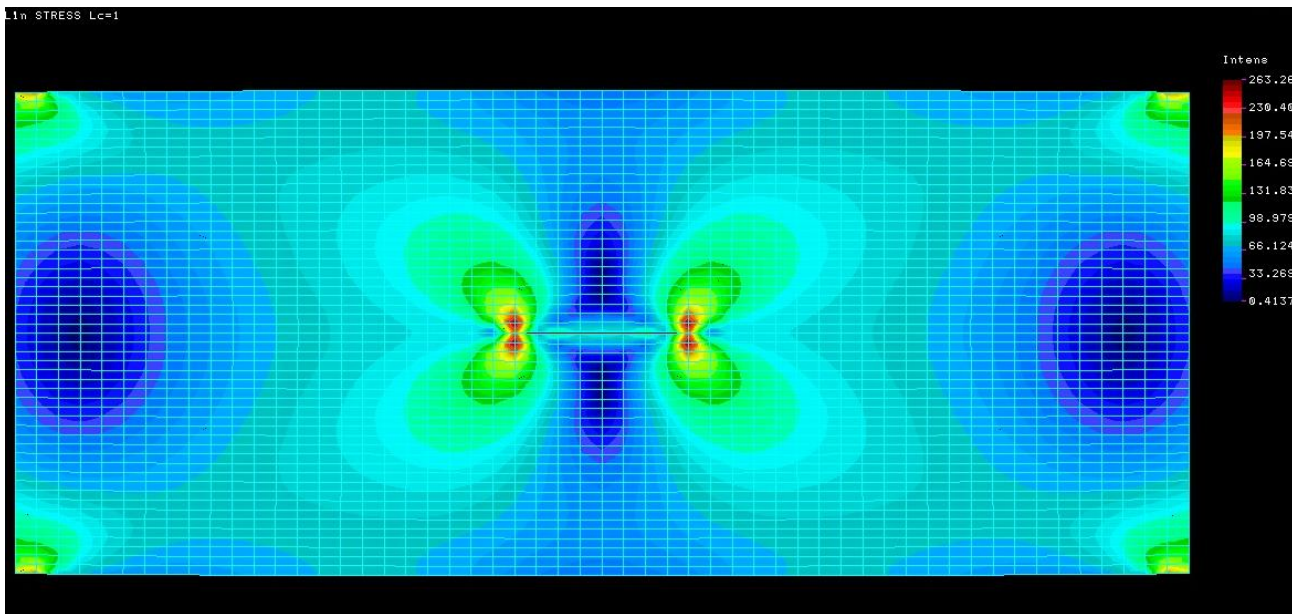

Fig. 3.10 Stress Intesity in Stage 4

Stage 5

L = L1 + L2 = 0.315 + 0.315 = 0.630 inch

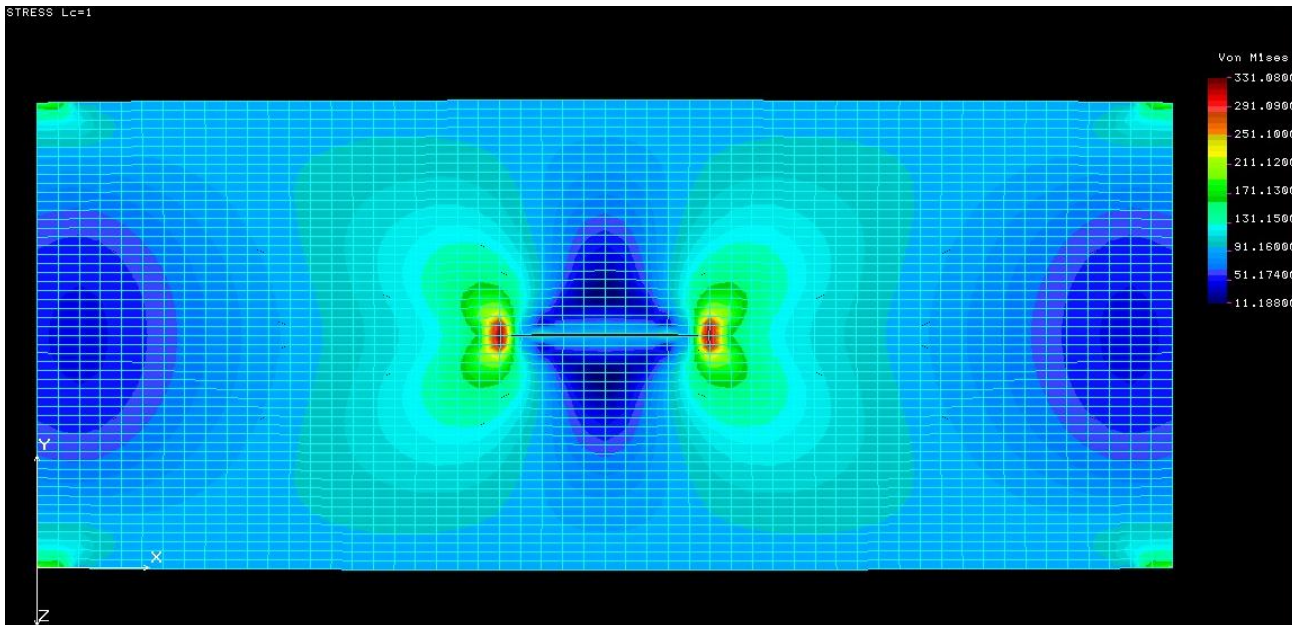

Fig. 3.11 Stress Von Mises in Stage 5

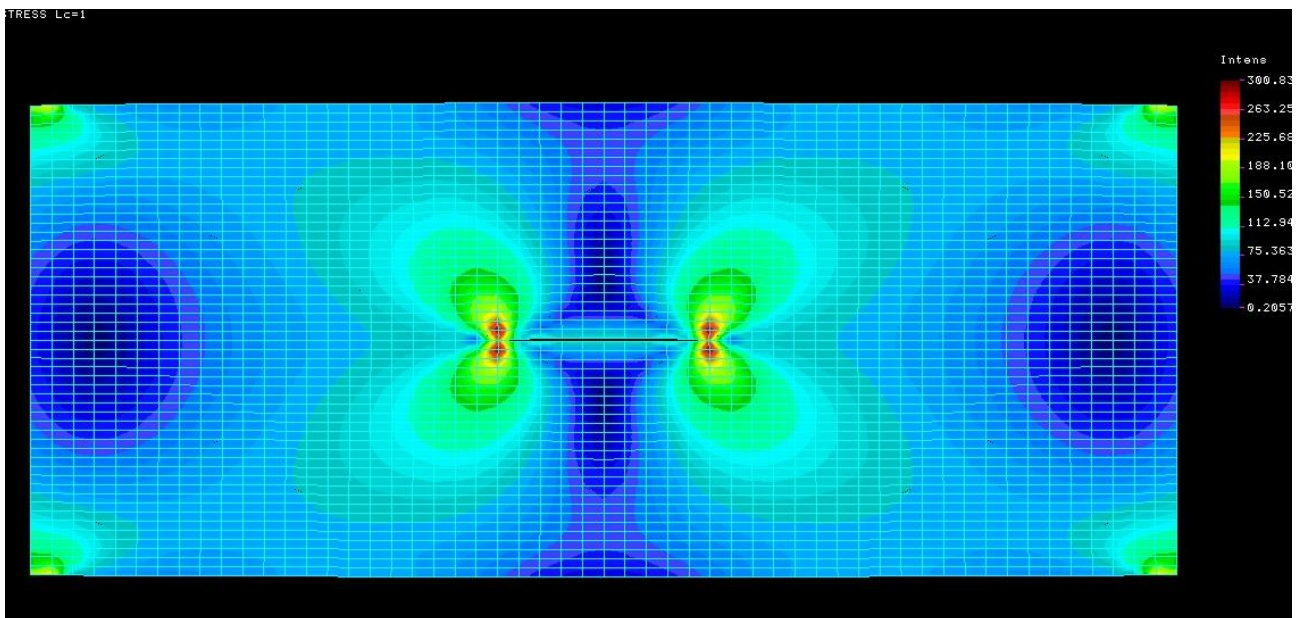
Fig. 3.12 Stress Intesity in Stage 5
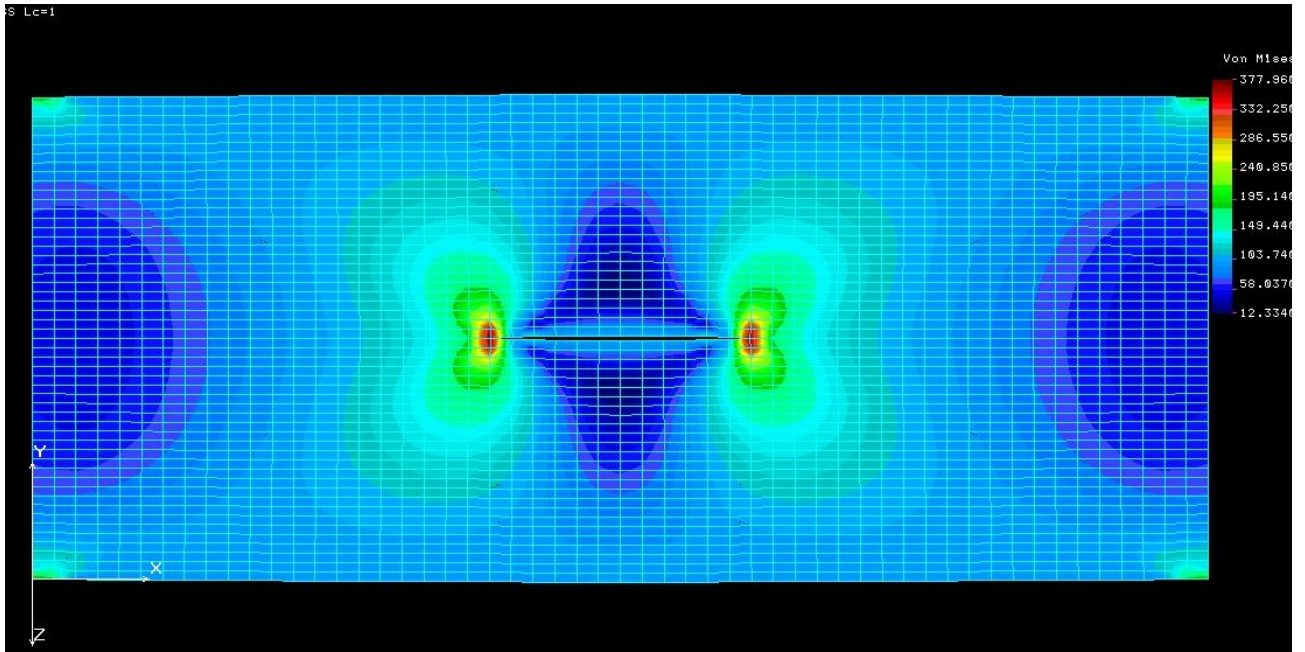
Stage 6

L = L1 + L2 = 0.378 + 0.378 = 0.756 inch

Fig. 3.13 Stress Von Mises in Stage 6

Fig. 3.14 Stress Intesity in Stage 6

Stage 7

L = L1 + L2 = 0.441 + 0.441 = 0.882 inch

Fig. 3.15 Stress Von Mises in Stage 7

Fig. 3.16 Stress Intesity in Stage 7

Stage 8

Li = L1 + L2 = 0.504 + 0.504 = 1.008 inch

Fig. 3.17 Stress Von Mises in Stage 8

Fig. 3.18 Stress Intesity in Stage 8

Stage 9

Li = L1 + L2 = 0.567 + 0.567 = 1.134 inch

Fig. 3.19 Stress Von Mises in Stage 9
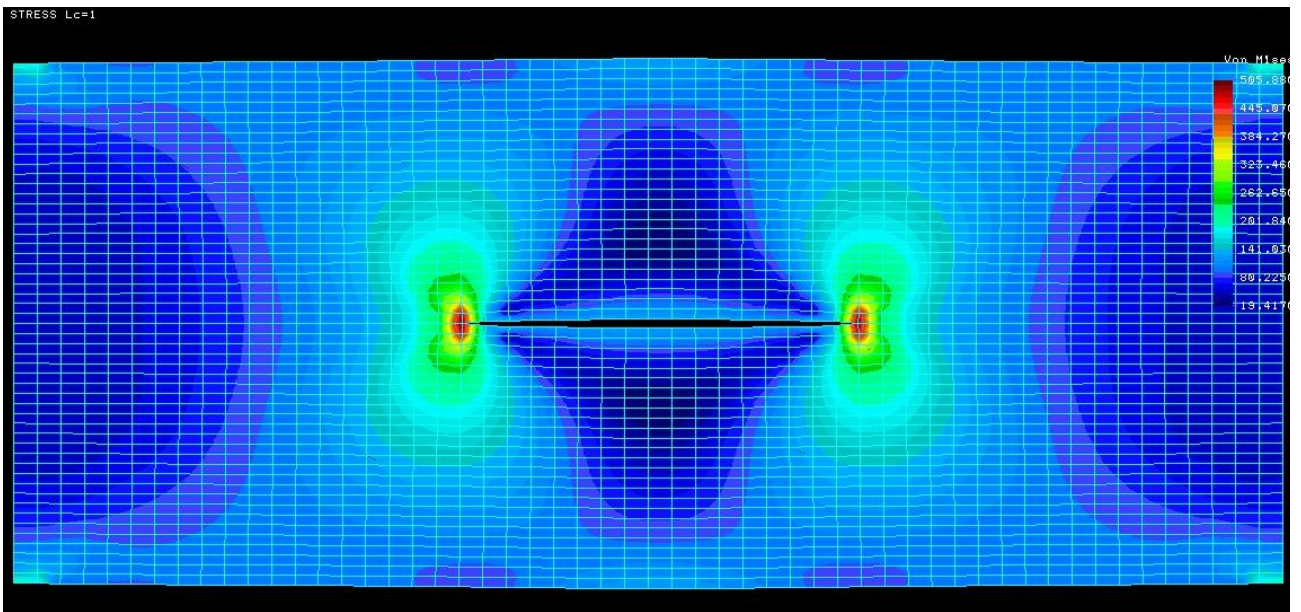
Fig. 3.20 Stress Intesity in Stage 9

Stage 10

Li = L1 + L2 = 0.63 + 0.63 = 1.26 inch
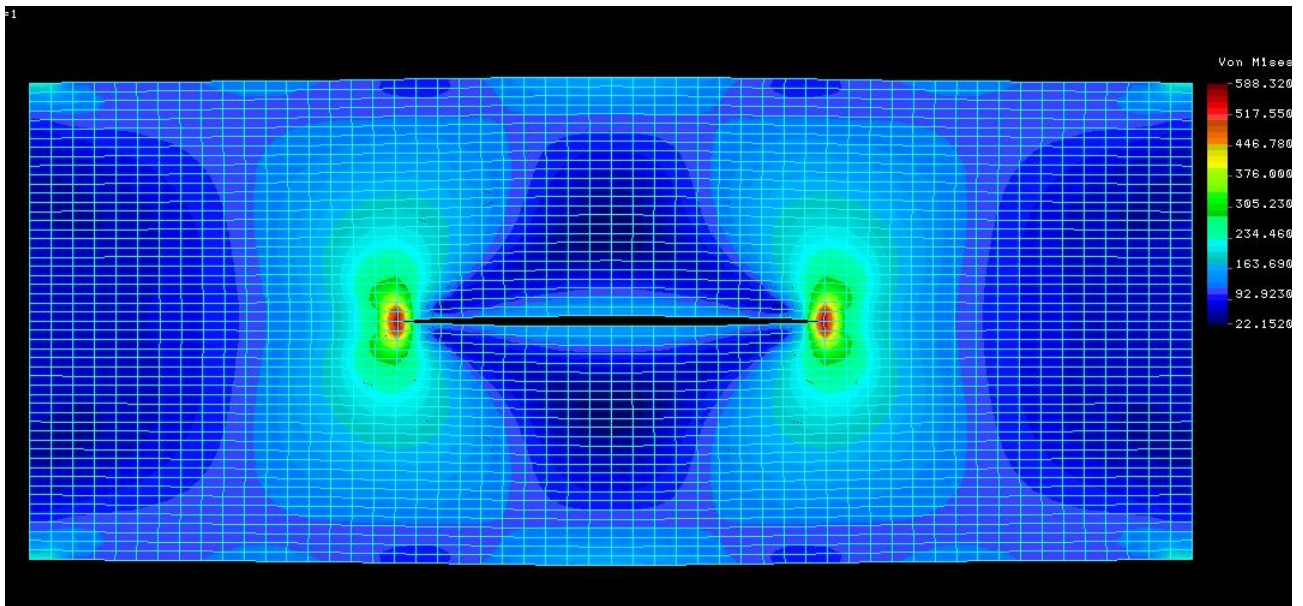
Fig. 3.21 Stress Von Mises in Stage 10

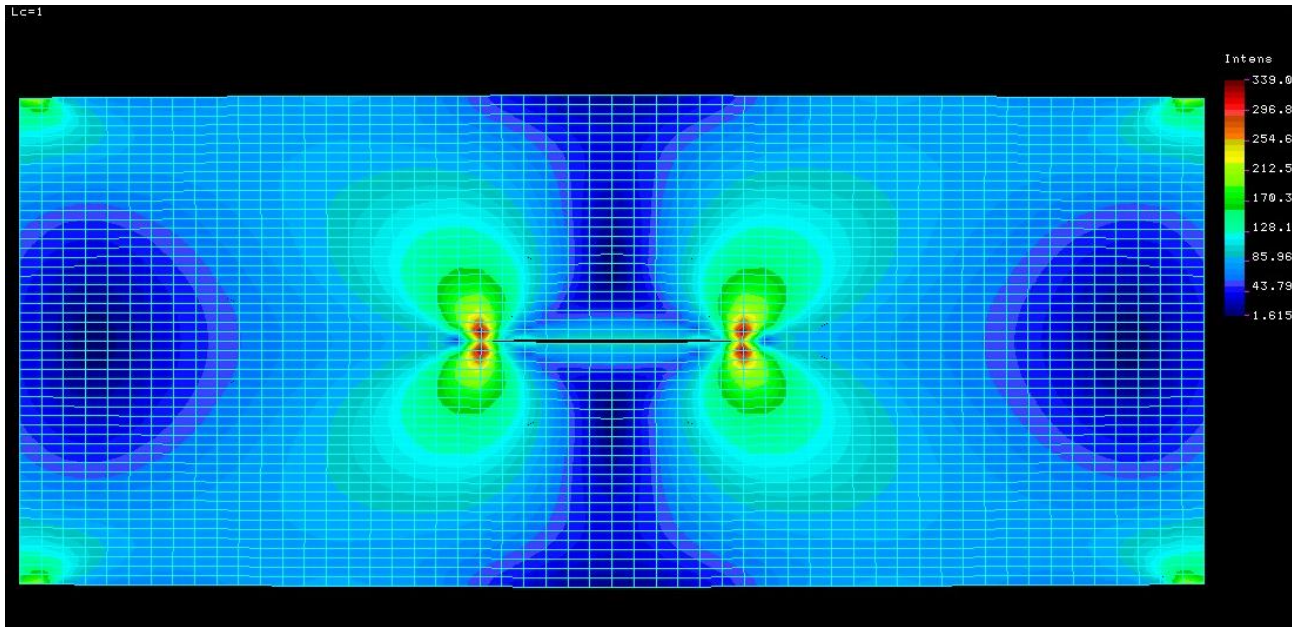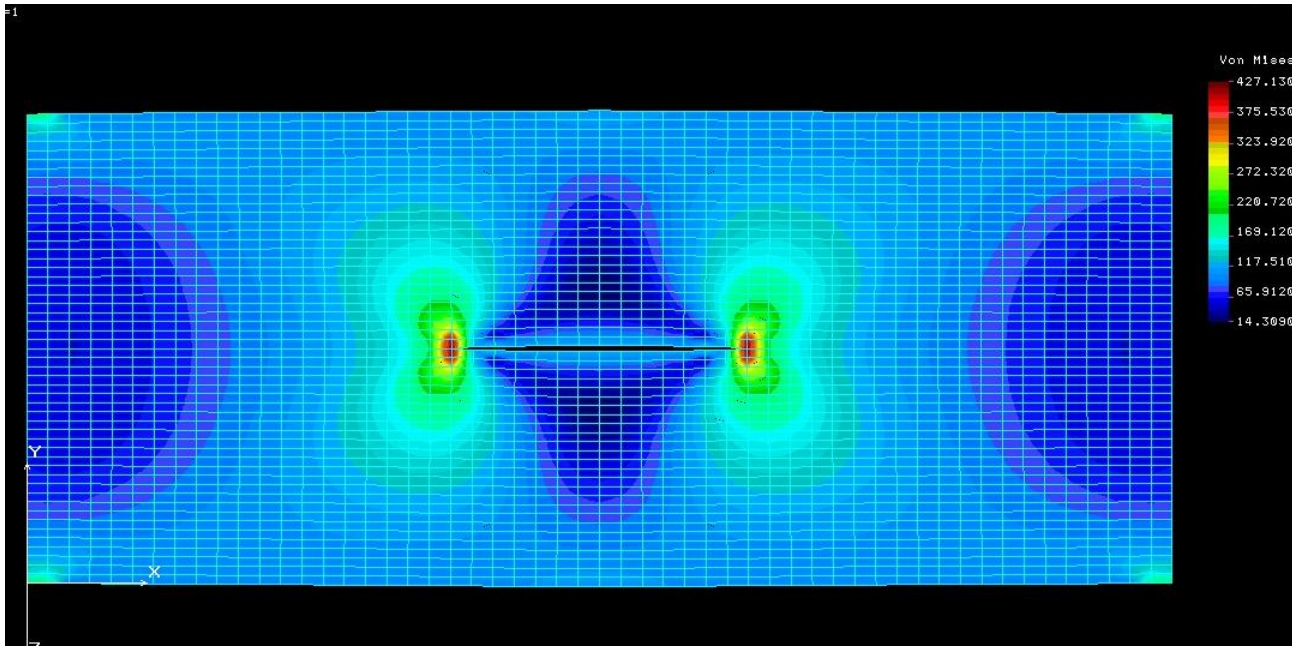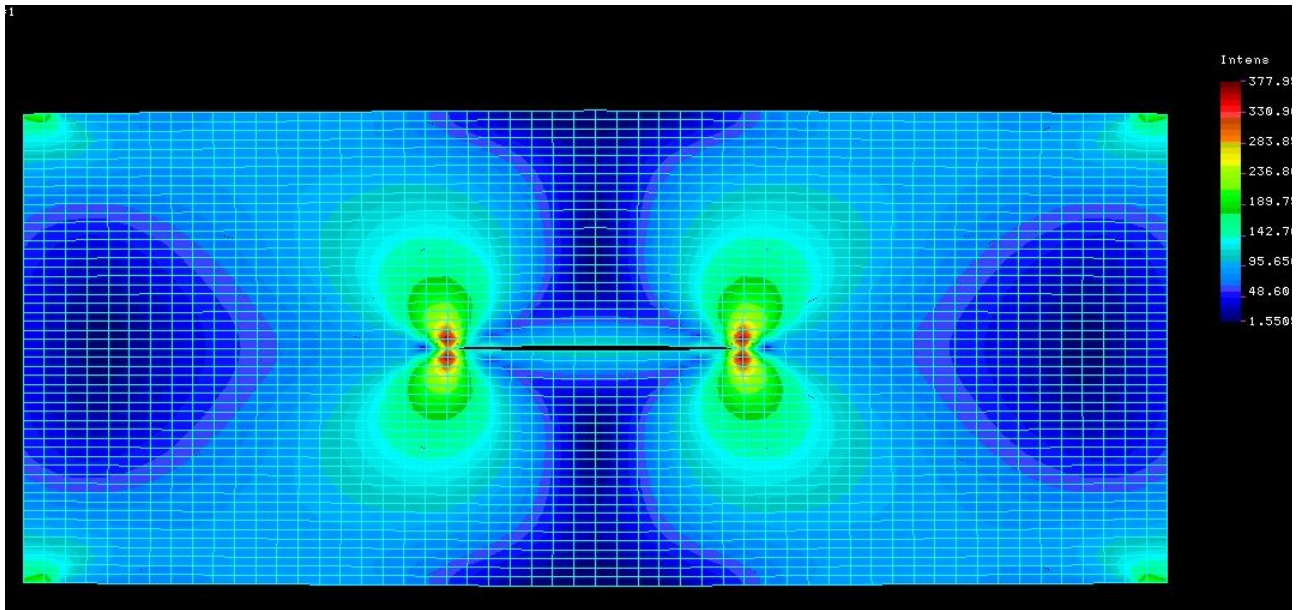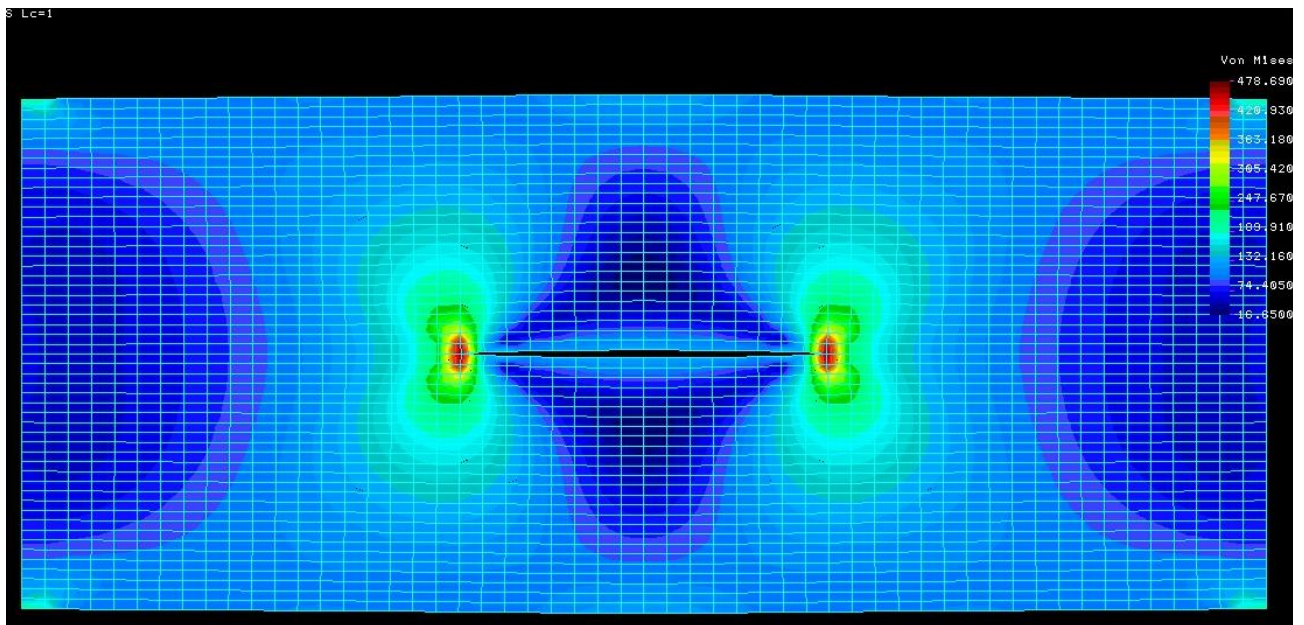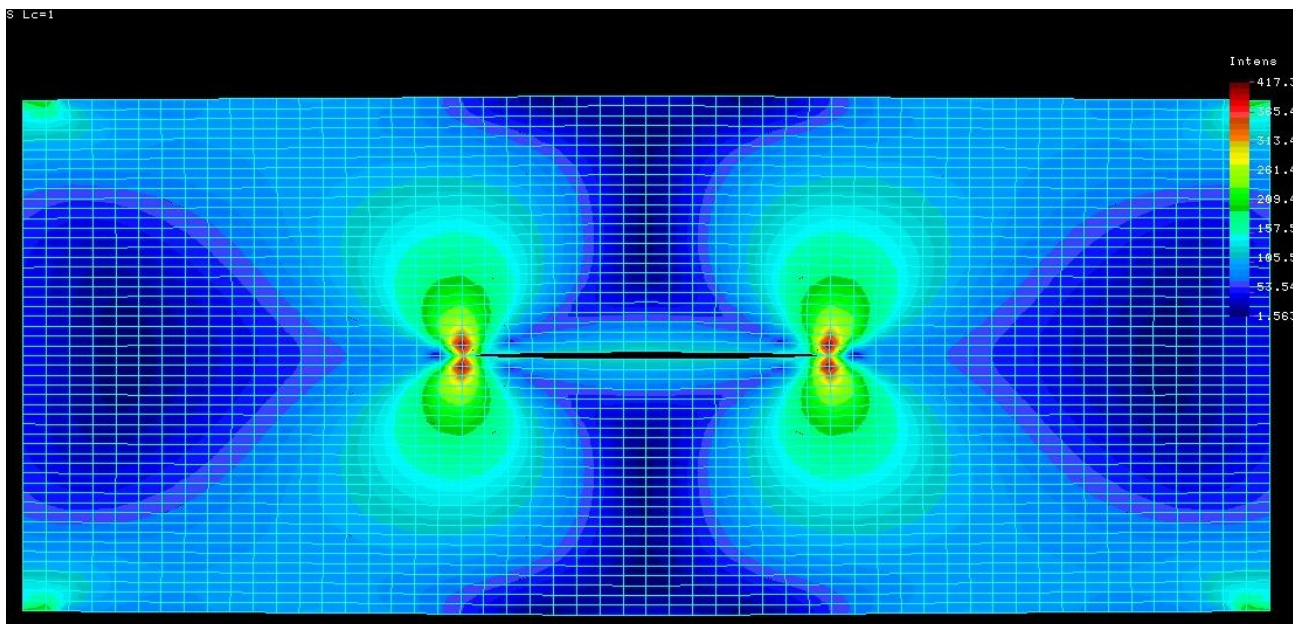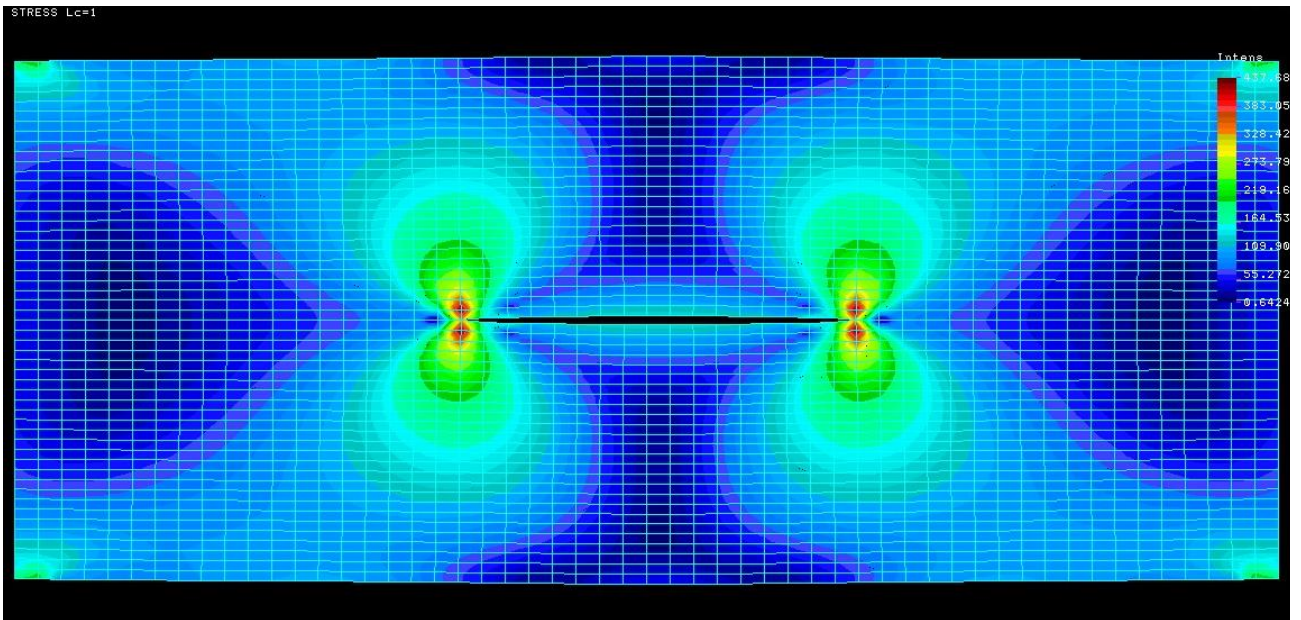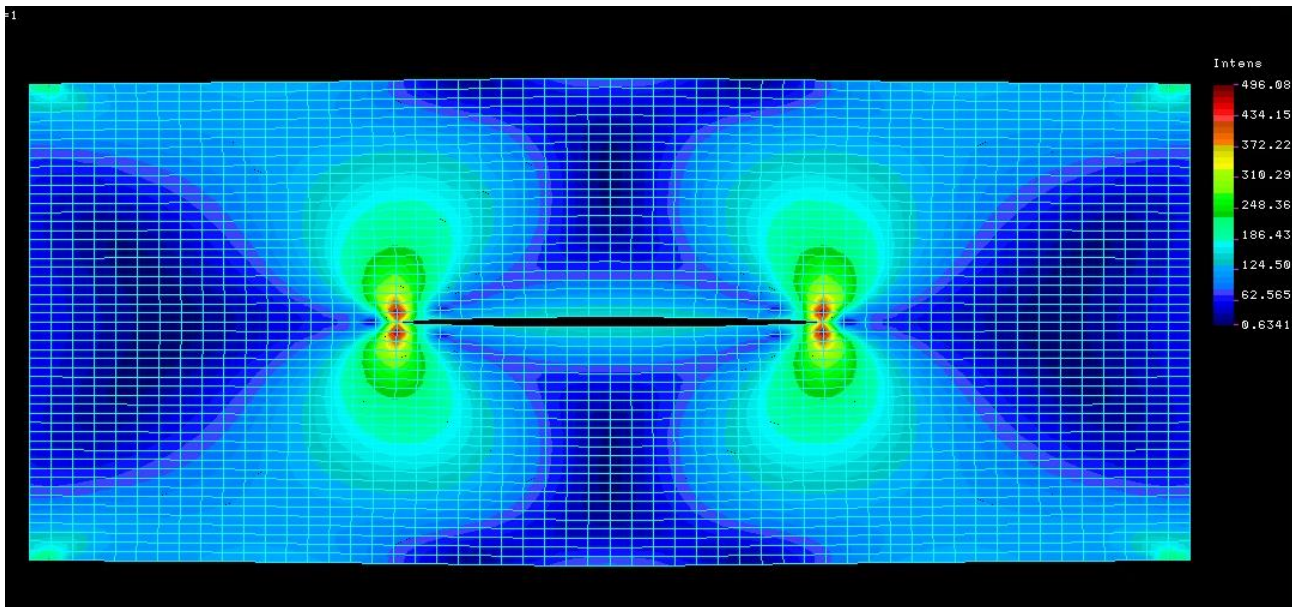Fig. 3.22 Stress Intesity in Stage 10

I got such results as Stress intensity factor and Stress von Mises for each stage of crack growth:

Table 3.1 Summary of results

Node	Ka, psi	Sigma, psi	l, in
1457	143.70	154.30	0.126
1456	162.40	197.40	0.252
1455	187.80	242.10	0.378
1454	213.30	286.10	0.504
1453	239.10	331.10	0.63
1452	265.20	378.00	0.756
1451	291.50	427.10	0.882
1450	317.60	478.70	1.008
1449	330.90	505.90	1.134
1448	367.30	588.30	1.26

Using the formula 2.1.7 we can calculate the Y-factor using Stress intensity factor and Stress von Mises:

Table 3.2 Calculate of a Y-factor

Ka	sigma	l	Y
143.7	154.3	0.126	1.480236
162.4	197.4	0.252	0.924621
187.8	242.1	0.378	0.711836
213.3	286.1	0.504	0.592493
239.1	331.1	0.63	0.513305
265.2	378	0.756	0.455246
291.5	427.1	0.882	0.410015
317.6	478.7	1.008	0.372831
330.9	505.9	1.134	0.346538
367.3	588.3	1.26	0.313807

Dependence of the SIF on the length of the crack l.

The dependence of Stress Intesity on crack length
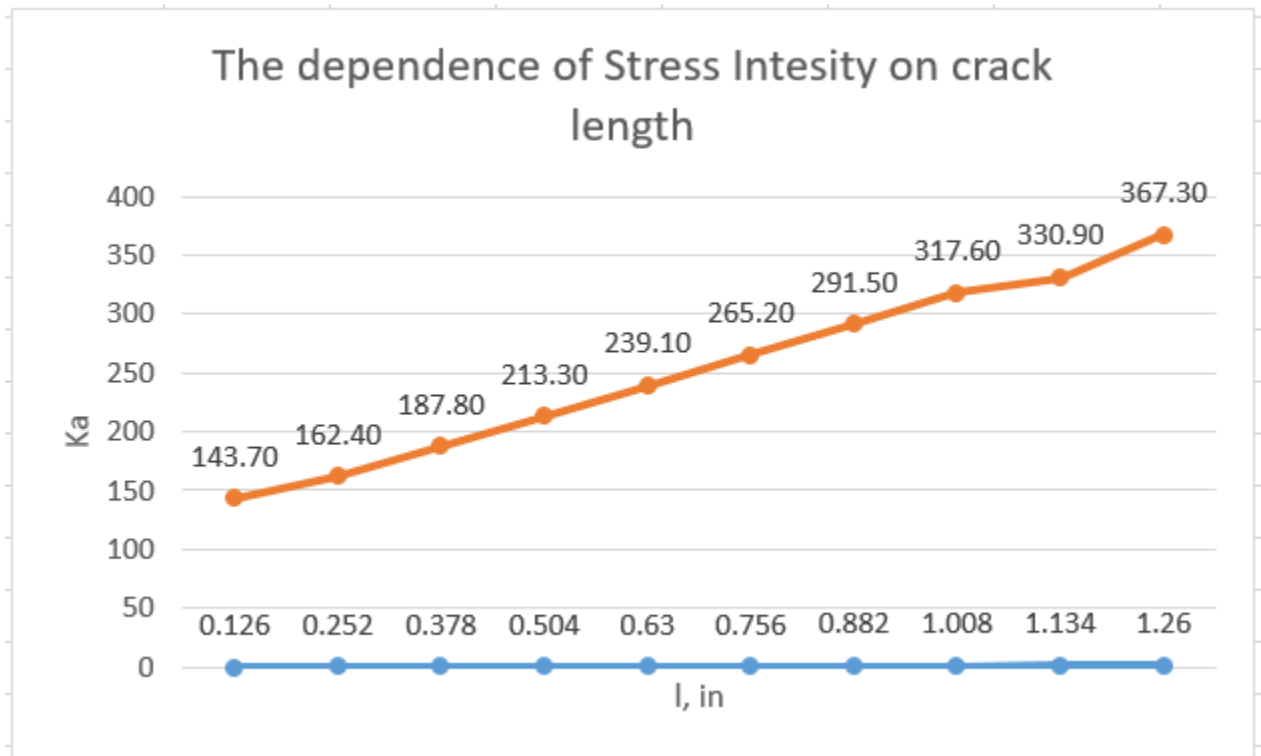
Dependence of the Y-factor on the length of the crack l.

The dependence of Geometric factor on crack length
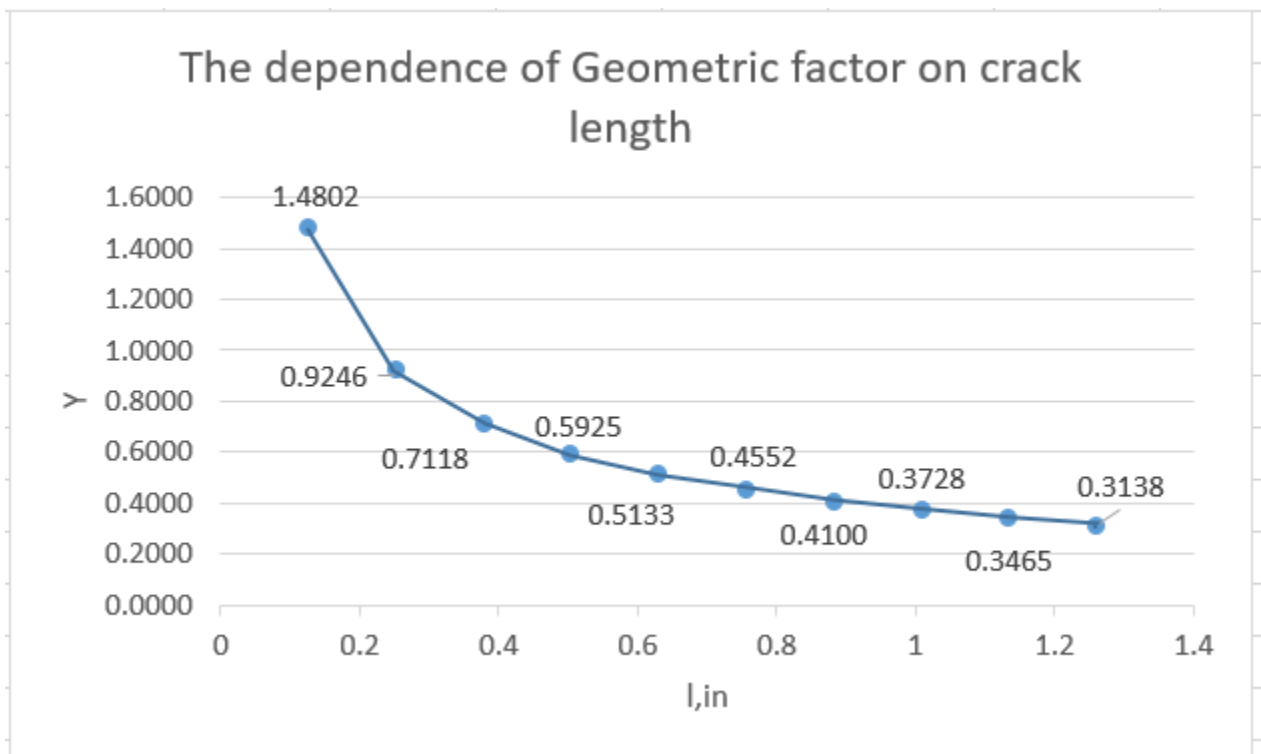
4. STARTUP DEVELOPMENT

The developed calculation method is universal for any aircraft structure and allows one to calculate crack growth using modern FEM packages that cannot predict crack growth, but can find the stress intensity factor at the crack tip, thus fully determining its behavior.

If you have the above data set, you can develop a calculation package that will predict crack behavior, which is very relevant for the analysis of modern aircraft structures

```
┌─────────────────────────────────────┐
│        Geometric parameters          │
│              Material                │
│               Loads                  │
│      Creck length in each stage      │
└─────────────────────────────────────┘
                  │
                  ▼
┌─────────────────────────────────────┐
│                                      │
│            FEM programm              │
│                                      │
└─────────────────────────────────────┘
                  │
                  ▼
┌─────────────────────────────────────┐
│               Stress                 │
│       Stress Intensity Factor        │
│        Predict crack behavior        │
└─────────────────────────────────────┘
```
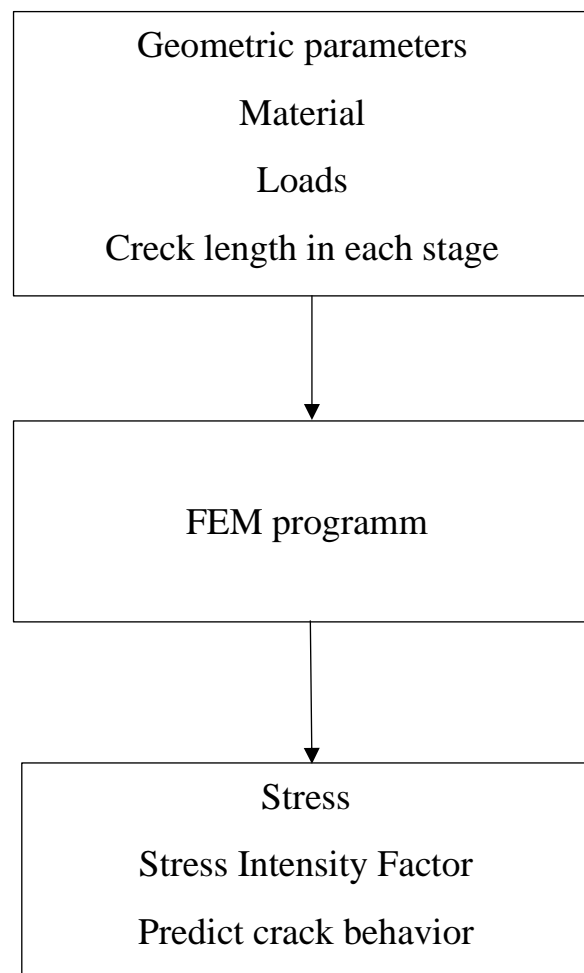
CONCLUSION

1. The developed calculation procedure allows predicting crack growth and its future behavior.

2. The analysis of the dependence of the coefficient of stress intensity on the length of the crack.

3. The dependence of the coefficient taking into account the geometric parameters of the plate on the crack length has been analyzed.

4. Knowing the obtained parameters (coefficient of stress intensity; coefficient taking into account the geometric parameters of the plate), inspection intervals can be set with the highest probability of crack detection.

REFERENCES

1. Federal Aviation Regulation (FAR) Part 25, Paragraph 25.571 – "Damage Tolerance and Fatigue Evaluation of Structures", U.S.A

2. David Broek, Elementary Engineering Fracture Mech, 1980. – 368 c.

3.Roberta Lazzeri Department of Aerospace Engineering Pisa University Via Diotisalvi, 2, 56126 Pisa, Italy

4. https://lessonslearned.faa.gov/

5. Orowan E.O. In: Proc, Symposium on internal stresses in metals and alloys , London: Instituteof Metals. – 1948. – P. 451.

6. Metallic Materials Properties Development and Standardization(MMPDS) DOT/FAA/AR-MMPDS-01- -Office of Aviation Research Washington, D.C. 20591

7. Mike Mohaghegh, Aircraft Structures Design and Analysis, San Diego, - 2008 – P25

APPENDIX A

Results

Stage 10

Stage 9

STRLIST,1,1,1,0,2,1,2970,1

Node	Princ_1	Princ_2	Load case Princ_3	1 Top Face Von_Mises	Layer 1 Intens
1447	1.656e+002	0.000e+000	9.348e+001	1.438e+002	7.207e+001
1448	2.015e+002	0.000e+000	1.133e+002	1.749e+002	8.824e+001
1449	2.299e+002	0.000e+000	2.223e+002	2.262e+002	7.596e+000
1450	5.506e+002	0.000e+000	2.330e+002	4.787e+002	3.176e+002
1451	2.170e+001	0.000e+000	-1.149e+002	1.272e+002	1.366e+002
1452	2.183e+001	0.000e+000	-1.255e+002	1.378e+002	1.474e+002
1453	-3.111e+000	0.000e+000	-1.052e+002	1.037e+002	1.021e+002
1454	9.174e-001	0.000e+000	-1.154e+002	1.158e+002	1.163e+002
1455	1.540e-001	0.000e+000	-1.176e+002	1.176e+002	1.177e+002
1456	1.736e-001	0.000e+000	-1.206e+002	1.207e+002	1.207e+002
1457	1.821e-001	0.000e+000	-1.221e+002	1.222e+002	1.223e+002
1458	1.595e-001	0.000e+000	-1.227e+002	1.228e+002	1.229e+002
1459	1.821e-001	0.000e+000	-1.221e+002	1.222e+002	1.223e+002
1460	1.736e-001	0.000e+000	-1.206e+002	1.207e+002	1.207e+002
1461	1.540e-001	0.000e+000	-1.176e+002	1.176e+002	1.177e+002
1462	9.174e-001	0.000e+000	-1.154e+002	1.158e+002	1.163e+002
1463	-3.111e+000	0.000e+000	-1.052e+002	1.037e+002	1.021e+002
1464	2.183e+001	0.000e+000	-1.255e+002	1.378e+002	1.474e+002
1465	2.169e+001	0.000e+000	-1.149e+002	1.272e+002	1.366e+002
1466	5.506e+002	0.000e+000	2.330e+002	4.787e+002	3.176e+002
1467	2.299e+002	0.000e+000	2.223e+002	2.262e+002	7.596e+000
1468	2.015e+002	0.000e+000	1.133e+002	1.749e+002	8.824e+001
1469	1.656e+002	0.000e+000	9.348e+001	1.438e+002	7.207e+001
1470	1.472e+002	0.000e+000	7.717e+001	1.275e+002	7.000e+001
1471	1.324e+002	0.000e+000	6.838e+001	1.147e+002	6.402e+001
1472	1.208e+002	0.000e+000	6.195e+001	1.046e+002	5.883e+001
1473	1.108e+002	0.000e+000	5.747e+001	9.599e+001	5.334e+001

Stage 8

STRLIST,1,1,1,0,2,1,2970,1

Node	Princ_1	Princ_2	Load case Princ_3	1 Top Face Von_Mises	Layer 1 Intens
1444	1.112e+002	0.000e+000	4.933e+001	9.652e+001	6.188e+001
1445	1.194e+002	0.000e+000	5.309e+001	1.036e+002	6.632e+001
1446	1.289e+002	0.000e+000	5.849e+001	1.118e+002	7.045e+001
1447	1.411e+002	0.000e+000	6.587e+001	1.223e+002	7.523e+001
1448	1.562e+002	0.000e+000	7.976e+001	1.353e+002	7.648e+001
1449	1.866e+002	0.000e+000	9.648e+001	1.616e+002	9.013e+001
1450	2.099e+002	0.000e+000	1.916e+002	2.014e+002	1.828e+001
1451	4.903e+002	0.000e+000	1.988e+002	4.271e+002	2.915e+002
1452	1.216e+001	0.000e+000	-1.041e+002	1.107e+002	1.163e+002
1453	1.946e+001	0.000e+000	-1.197e+002	1.305e+002	1.391e+002
1454	-2.785e+000	0.000e+000	-1.005e+002	9.914e+001	9.772e+001
1455	8.178e-001	0.000e+000	-1.084e+002	1.088e+002	1.092e+002
1456	1.372e-001	0.000e+000	-1.093e+002	1.093e+002	1.094e+002
1457	1.513e-001	0.000e+000	-1.108e+002	1.109e+002	1.110e+002
1458	1.720e-001	0.000e+000	-1.112e+002	1.113e+002	1.113e+002
1459	1.513e-001	0.000e+000	-1.108e+002	1.109e+002	1.110e+002
1460	1.372e-001	0.000e+000	-1.093e+002	1.093e+002	1.094e+002
1461	8.178e-001	0.000e+000	-1.084e+002	1.088e+002	1.092e+002
1462	-2.785e+000	0.000e+000	-1.005e+002	9.914e+001	9.772e+001
1463	1.946e+001	0.000e+000	-1.197e+002	1.305e+002	1.391e+002
1464	1.217e+001	0.000e+000	-1.041e+002	1.107e+002	1.163e+002
1465	4.903e+002	0.000e+000	1.988e+002	4.271e+002	2.915e+002
1466	2.099e+002	0.000e+000	1.916e+002	2.014e+002	1.828e+001
1467	1.866e+002	0.000e+000	9.648e+001	1.616e+002	9.013e+001
1468	1.562e+002	0.000e+000	7.976e+001	1.353e+002	7.648e+001
1469	1.411e+002	0.000e+000	6.587e+001	1.223e+002	7.523e+001
1470	1.289e+002	0.000e+000	5.849e+001	1.118e+002	7.045e+001
1471	1.194e+002	0.000e+000	5.309e+001	1.036e+002	6.632e+001
1472	1.112e+002	0.000e+000	4.933e+001	9.652e+001	6.188e+001
1473	1.039e+002	0.000e+000	4.655e+001	9.013e+001	5.734e+001
1474	9.705e+001	0.000e+000	4.454e+001	8.414e+001	5.251e+001

Stage 7

STRLIST,1,1,1,0,2,1,2970,1

Node	Princ_1	Princ_2	Load case Princ_3	1 Top Face Von_Mises	Layer 1 Intens
1450	1.720e+002	0.000e+000	8.168e+001	1.490e+002	9.029e+001
1451	1.905e+002	0.000e+000	1.637e+002	1.786e+002	2.686e+001
1452	4.328e+002	0.000e+000	1.676e+002	3.780e+002	2.652e+002
1453	4.384e+000	0.000e+000	-9.368e+001	9.595e+001	9.807e+001
1454	1.719e+001	0.000e+000	-1.129e+002	1.224e+002	1.301e+002
1455	-2.467e+000	0.000e+000	-9.502e+001	9.381e+001	9.256e+001
1456	7.216e-001	0.000e+000	-1.011e+002	1.015e+002	1.018e+002
1457	1.307e-001	0.000e+000	-1.009e+002	1.010e+002	1.011e+002
1458	1.433e-001	0.000e+000	-1.016e+002	1.017e+002	1.017e+002
1459	1.307e-001	0.000e+000	-1.009e+002	1.010e+002	1.011e+002
1460	7.216e-001	0.000e+000	-1.011e+002	1.015e+002	1.018e+002
1461	-2.467e+000	0.000e+000	-9.502e+001	9.381e+001	9.256e+001
1462	1.719e+001	0.000e+000	-1.129e+002	1.224e+002	1.301e+002
1463	4.384e+000	0.000e+000	-9.368e+001	9.595e+001	9.807e+001
1464	4.328e+002	0.000e+000	1.676e+002	3.780e+002	2.652e+002
1465	1.905e+002	0.000e+000	1.637e+002	1.786e+002	2.686e+001
1466	1.720e+002	0.000e+000	8.168e+001	1.490e+002	9.029e+001
1467	1.468e+002	0.000e+000	6.780e+001	1.273e+002	7.900e+001
1468	1.347e+002	0.000e+000	5.617e+001	1.172e+002	7.850e+001
1469	1.249e+002	0.000e+000	5.008e+001	1.089e+002	7.485e+001
1470	1.173e+002	0.000e+000	4.563e+001	1.025e+002	7.172e+001
1471	1.108e+002	0.000e+000	4.253e+001	9.682e+001	6.828e+001
1472	1.049e+002	0.000e+000	4.022e+001	9.168e+001	6.469e+001
1473	9.936e+001	0.000e+000	3.854e+001	8.677e+001	6.082e+001
1474	9.391e+001	0.000e+000	3.737e+001	8.190e+001	5.655e+001
1475	8.841e+001	0.000e+000	3.667e+001	7.693e+001	5.174e+001
1476	8.270e+001	0.000e+000	3.644e+001	7.179e+001	4.626e+001
1477	7.669e+001	0.000e+000	3.669e+001	6.643e+001	3.999e+001

Stage 6

STRLIST,1,1,1,0,2,1,2970,1

Node	Princ_1	Princ_2	Load case Princ_3	1 Top Face Von_Mises	Layer 1 Intens
1447	1.147e+002	0.000e+000	3.942e+001	1.010e+002	7.529e+001
1448	1.205e+002	0.000e+000	4.301e+001	1.058e+002	7.750e+001
1449	1.280e+002	0.000e+000	4.789e+001	1.120e+002	8.011e+001
1450	1.374e+002	0.000e+000	5.741e+001	1.195e+002	7.996e+001
1451	1.577e+002	0.000e+000	6.862e+001	1.370e+002	8.908e+001
1452	1.718e+002	0.000e+000	1.381e+002	1.577e+002	3.377e+001
1453	3.779e+002	0.000e+000	1.388e+002	3.311e+002	2.391e+002
1454	-2.043e+000	0.000e+000	-8.384e+001	8.284e+001	8.180e+001
1455	1.502e+001	0.000e+000	-1.058e+002	1.140e+002	1.208e+002
1456	-2.152e+000	0.000e+000	-8.939e+001	8.833e+001	8.724e+001
1457	6.417e-001	0.000e+000	-9.407e+001	9.439e+001	9.471e+001
1458	9.668e-002	0.000e+000	-9.311e+001	9.316e+001	9.321e+001
1459	6.417e-001	0.000e+000	-9.407e+001	9.439e+001	9.471e+001
1460	-2.152e+000	0.000e+000	-8.939e+001	8.833e+001	8.724e+001
1461	1.502e+001	0.000e+000	-1.058e+002	1.140e+002	1.208e+002
1462	-2.043e+000	0.000e+000	-8.384e+001	8.284e+001	8.180e+001
1463	3.779e+002	0.000e+000	1.388e+002	3.311e+002	2.391e+002
1464	1.718e+002	0.000e+000	1.381e+002	1.577e+002	3.377e+001
1465	1.577e+002	0.000e+000	6.862e+001	1.370e+002	8.908e+001
1466	1.374e+002	0.000e+000	5.741e+001	1.195e+002	7.996e+001
1467	1.280e+002	0.000e+000	4.789e+001	1.120e+002	8.011e+001
1468	1.205e+002	0.000e+000	4.301e+001	1.058e+002	7.750e+001
1469	1.147e+002	0.000e+000	3.942e+001	1.010e+002	7.529e+001
1470	1.097e+002	0.000e+000	3.693e+001	9.668e+001	7.277e+001

Stage 5

STRLIST,1,1,1,0,2,1,2970,1

Node	Princ_1	Princ_2	Princ_3	Load case 1 Top Face Von_Mises	Layer 1 Intens
1444	9.812e+001	0.000e+000	2.903e+001	8.731e+001	6.909e+001
1445	1.014e+002	0.000e+000	2.984e+001	9.030e+001	7.161e+001
1446	1.047e+002	0.000e+000	3.095e+001	9.317e+001	7.376e+001
1447	1.080e+002	0.000e+000	3.242e+001	9.603e+001	7.562e+001
1448	1.117e+002	0.000e+000	3.435e+001	9.906e+001	7.732e+001
1449	1.158e+002	0.000e+000	3.713e+001	1.024e+002	7.871e+001
1450	1.213e+002	0.000e+000	4.089e+001	1.069e+002	8.040e+001
1451	1.281e+002	0.000e+000	4.839e+001	1.121e+002	7.973e+001
1452	1.439e+002	0.000e+000	5.702e+001	1.255e+002	8.691e+001
1453	1.539e+002	0.000e+000	1.143e+002	1.384e+002	3.964e+001
1454	3.251e+002	0.000e+000	1.118e+002	2.861e+002	2.133e+002
1455	-7.525e+000	0.000e+000	-7.470e+001	7.123e+001	6.717e+001
1456	1.294e+001	0.000e+000	-9.884e+001	1.059e+002	1.118e+002
1457	-1.871e+000	0.000e+000	-8.407e+001	8.315e+001	8.220e+001
1458	1.001e+000	0.000e+000	-8.845e+001	8.896e+001	8.946e+001
1459	-1.871e+000	0.000e+000	-8.407e+001	8.315e+001	8.220e+001
1460	1.294e+001	0.000e+000	-9.884e+001	1.059e+002	1.118e+002
1461	-7.525e+000	0.000e+000	-7.470e+001	7.123e+001	6.717e+001
1462	3.251e+002	0.000e+000	1.118e+002	2.861e+002	2.133e+002
1463	1.539e+002	0.000e+000	1.143e+002	1.384e+002	3.964e+001
1464	1.439e+002	0.000e+000	5.702e+001	1.255e+002	8.691e+001
1465	1.281e+002	0.000e+000	4.839e+001	1.121e+002	7.973e+001
1466	1.213e+002	0.000e+000	4.089e+001	1.069e+002	8.040e+001
1467	1.158e+002	0.000e+000	3.713e+001	1.024e+002	7.871e+001

Stage 4

STRLIST,1,1,1,0,2,1,2970,1

Node	Princ_1	Princ_2	Princ_3	Load case 1 Top Face Von_Mises	Layer 1 Intens
1451	1.148e+002	0.000e+000	3.500e+001	1.019e+002	7.977e+001
1452	1.193e+002	0.000e+000	4.052e+001	1.051e+002	7.878e+001
1453	1.308e+002	0.000e+000	4.655e+001	1.148e+002	8.425e+001
1454	1.369e+002	0.000e+000	9.160e+001	1.208e+002	4.527e+001
1455	2.732e+002	0.000e+000	8.538e+001	2.421e+002	1.878e+002
1456	-1.236e+001	0.000e+000	-6.644e+001	6.120e+001	5.408e+001
1457	1.125e+001	0.000e+000	-9.309e+001	9.920e+001	1.043e+002
1458	-3.241e+000	0.000e+000	-7.768e+001	7.612e+001	7.444e+001
1459	1.125e+001	0.000e+000	-9.309e+001	9.920e+001	1.043e+002
1460	-1.236e+001	0.000e+000	-6.644e+001	6.120e+001	5.408e+001
1461	2.732e+002	0.000e+000	8.538e+001	2.421e+002	1.878e+002
1462	1.369e+002	0.000e+000	9.160e+001	1.208e+002	4.527e+001
1463	1.308e+002	0.000e+000	4.655e+001	1.148e+002	8.425e+001
1464	1.193e+002	0.000e+000	4.052e+001	1.051e+002	7.878e+001
1465	1.148e+002	0.000e+000	3.500e+001	1.019e+002	7.977e+001
1466	1.111e+002	0.000e+000	3.232e+001	9.903e+001	7.883e+001
1467	1.084e+002	0.000e+000	3.031e+001	9.689e+001	7.812e+001
1468	1.060e+002	0.000e+000	2.889e+001	9.494e+001	7.713e+001
1469	1.038e+002	0.000e+000	2.779e+001	9.304e+001	7.598e+001
1470	1.015e+002	0.000e+000	2.693e+001	9.107e+001	7.456e+001
1471	9.909e+001	0.000e+000	2.628e+001	8.891e+001	7.281e+001
1472	9.645e+001	0.000e+000	2.583e+001	8.648e+001	7.062e+001
1473	9.348e+001	0.000e+000	2.559e+001	8.368e+001	6.789e+001
1474	9.010e+001	0.000e+000	2.561e+001	8.041e+001	6.448e+001
1475	8.621e+001	0.000e+000	2.593e+001	7.661e+001	6.028e+001
1476	8.175e+001	0.000e+000	2.659e+001	7.223e+001	5.517e+001
1477	7.666e+001	0.000e+000	2.763e+001	6.725e+001	4.903e+001
1478	7.090e+001	0.000e+000	2.908e+001	6.173e+001	4.181e+001
1479	6.446e+001	0.000e+000	3.098e+001	5.584e+001	3.349e+001

Stage 3

STRLIST,1,1,1,0,2,1,2970,1

			Load case	1 Top Face	Layer 1
Node	Princ_1	Princ_2	Princ_3	Von_Mises	Intens
1450	1.053e+002	0.000e+000	2.724e+001	9.470e+001	7.809e+001
1451	1.068e+002	0.000e+000	2.852e+001	9.580e+001	7.830e+001
1452	1.088e+002	0.000e+000	3.012e+001	9.733e+001	7.871e+001
1453	1.113e+002	0.000e+000	3.362e+001	9.883e+001	7.763e+001
1454	1.185e+002	0.000e+000	3.691e+001	1.051e+002	8.164e+001
1455	1.206e+002	0.000e+000	6.887e+001	1.048e+002	5.172e+001
1456	2.197e+002	0.000e+000	5.728e+001	1.974e+002	1.624e+002
1457	-1.710e+001	0.000e+000	-5.882e+001	5.240e+001	4.171e+001
1458	1.734e+001	0.000e+000	-9.542e+001	1.052e+002	1.128e+002
1459	-1.710e+001	0.000e+000	-5.882e+001	5.240e+001	4.171e+001
1460	2.197e+002	0.000e+000	5.728e+001	1.974e+002	1.624e+002
1461	1.206e+002	0.000e+000	6.887e+001	1.048e+002	5.172e+001
1462	1.185e+002	0.000e+000	3.691e+001	1.051e+002	8.164e+001
1463	1.113e+002	0.000e+000	3.362e+001	9.883e+001	7.763e+001
1464	1.088e+002	0.000e+000	3.012e+001	9.733e+001	7.871e+001
1465	1.068e+002	0.000e+000	2.852e+001	9.580e+001	7.830e+001
1466	1.053e+002	0.000e+000	2.724e+001	9.470e+001	7.809e+001
1467	1.040e+002	0.000e+000	2.631e+001	9.363e+001	7.766e+001
1468	1.026e+002	0.000e+000	2.554e+001	9.253e+001	7.708e+001
1469	1.012e+002	0.000e+000	2.491e+001	9.131e+001	7.627e+001
1470	9.955e+001	0.000e+000	2.439e+001	8.987e+001	7.516e+001
1471	9.767e+001	0.000e+000	2.400e+001	8.816e+001	7.367e+001
1472	9.546e+001	0.000e+000	2.376e+001	8.607e+001	7.169e+001
1473	9.283e+001	0.000e+000	2.371e+001	8.354e+001	6.912e+001
1474	8.972e+001	0.000e+000	2.389e+001	8.048e+001	6.583e+001
1475	8.605e+001	0.000e+000	2.435e+001	7.683e+001	6.170e+001
1476	8.175e+001	0.000e+000	2.513e+001	7.253e+001	5.662e+001
1477	7.677e+001	0.000e+000	2.629e+001	6.758e+001	5.048e+001
1478	7.109e+001	0.000e+000	2.785e+001	6.204e+001	4.323e+001
1479	6.469e+001	0.000e+000	2.985e+001	5.608e+001	3.485e+001
1480	5.763e+001	0.000e+000	3.226e+001	5.002e+001	2.537e+001
1481	4.996e+001	0.000e+000	3.507e+001	4.443e+001	1.490e+001

Stage 2

STRLIST,1,1,1,0,2,1,2970,1

			Load case	1 Top Face	Layer 1
Node	Princ_1	Princ_2	Princ_3	Von_Mises	Intens
1442	8.954e+001	0.000e+000	2.296e+001	8.056e+001	6.659e+001
1443	9.251e+001	0.000e+000	2.270e+001	8.351e+001	6.981e+001
1444	9.495e+001	0.000e+000	2.265e+001	8.590e+001	7.230e+001
1445	9.694e+001	0.000e+000	2.278e+001	8.780e+001	7.416e+001
1446	9.854e+001	0.000e+000	2.304e+001	8.928e+001	7.551e+001
1447	9.983e+001	0.000e+000	2.338e+001	9.043e+001	7.644e+001
1448	1.009e+002	0.000e+000	2.380e+001	9.131e+001	7.706e+001
1449	1.017e+002	0.000e+000	2.425e+001	9.198e+001	7.743e+001
1450	1.024e+002	0.000e+000	2.474e+001	9.250e+001	7.762e+001
1451	1.029e+002	0.000e+000	2.524e+001	9.293e+001	7.770e+001
1452	1.035e+002	0.000e+000	2.586e+001	9.328e+001	7.762e+001
1453	1.042e+002	0.000e+000	2.646e+001	9.380e+001	7.773e+001
1454	1.048e+002	0.000e+000	2.798e+001	9.397e+001	7.680e+001
1455	1.080e+002	0.000e+000	2.824e+001	9.702e+001	7.977e+001
1456	1.052e+002	0.000e+000	4.558e+001	9.136e+001	5.961e+001
1457	1.631e+002	0.000e+000	1.937e+001	1.543e+002	1.437e+002
1458	-2.522e+001	0.000e+000	-4.814e+001	4.171e+001	2.293e+001
1459	1.631e+002	0.000e+000	1.937e+001	1.543e+002	1.437e+002
1460	1.052e+002	0.000e+000	4.558e+001	9.136e+001	5.961e+001
1461	1.080e+002	0.000e+000	2.824e+001	9.702e+001	7.977e+001
1462	1.048e+002	0.000e+000	2.798e+001	9.397e+001	7.680e+001
1463	1.042e+002	0.000e+000	2.646e+001	9.380e+001	7.773e+001
1464	1.035e+002	0.000e+000	2.586e+001	9.328e+001	7.762e+001
1465	1.029e+002	0.000e+000	2.524e+001	9.293e+001	7.770e+001
1466	1.024e+002	0.000e+000	2.474e+001	9.250e+001	7.762e+001
1467	1.017e+002	0.000e+000	2.425e+001	9.198e+001	7.743e+001
1468	1.009e+002	0.000e+000	2.380e+001	9.131e+001	7.706e+001
1469	9.983e+001	0.000e+000	2.338e+001	9.043e+001	7.644e+001
1470	9.854e+001	0.000e+000	2.304e+001	8.928e+001	7.551e+001
1471	9.694e+001	0.000e+000	2.278e+001	8.780e+001	7.416e+001

Stage 1